(2)

The Deposition of Multicomponent Films for Electrooptic Applications via a Computer Controlled Dual Ion Beam Sputtering System

ONR Contract No. N00014-88-K-0526

Final Project Report
Covering the period July 1, 1988 - Dec. 31, 1991

Principal Investigators:

Angus I. Kingon **Orlando Auciello** **Klaus J. Bachmann**

North Carolina State University
Department of Materials Science and Engineering
Raleigh, NC 27695-7907
(919) 515-2867

This contract report was prepared by Dr. T. M. Graettinger.

The views and conclusions contained in this document are those of the authors and should not be interpreted as necessarily representing the official policies, either expressed or implied, of the Office of Naval Research or the U. S. Government.

TABLE OF CONTENTS

PROJECT SUMMARY

This is the final report covering our 3-year Office of Naval Research contract N00014-88-K-0526. The original program goals included:

1) Deposition of potassium niobate, $KNbO_3$, thin films using a computer-controlled ion beam sputter-deposition system.
2) Investigation of critical process parameters and their relationship to film properties.
3) Characterization of the optical and electro-optical properties of $KNbO_3$ thin films.

ACCOMPLISHMENTS

Presented here is a summary of project accomplishments which are described in detail in this report.

1) Development of a computer-controlled ion beam sputter-deposition system for the in situ growth of multicomponent oxide thin films.

A novel ion beam sputter-deposition method was developed to deposit $KNbO_3$ and other multicomponent thin films in a high vacuum chamber. The method involves layer by layer growth of the multicomponent material. The uniqueness of the system lies in a rotating target holder and the process monitoring and control. The technique requires that multiple targets be sequentially exposed to the ion beam. An in-vacuum, motor-driven rotating target holder was built to perform this function. The targets are either elemental materials (e.g. niobium metal, Nb) or elemental oxides (e.g. potassium superoxide, KO_2). Also central to the deposition process is real-time feedback from a quartz crystal resonator, QCR, whose frequency changes in response to material deposited on the quartz crystal surface. For system control, the QCR actively senses deposition during the sputtering process and when preset values are reached its signal triggers target rotation via the system control computer. The computer also performs many other system functions including control of ion beam parameters and substrate heating.

At sufficiently high deposition temperatures the deposited layers interdiffuse to form the desired multicomponent material. Cation

stoichiometry has been precisely controlled by adjusting the relative thicknesses of the deposited layers.

2) Deposition and microstructural characterization of $KNbO_3$ thin films.

Prior to this investigation, little work had been done to fabricate high quality thin films of $KNbO_3$. Thus, little was known about the microstructural characteristics of $KNbO_3$ thin films. In order to produce the highest quality films possible, single crystal materials were chosen as substrates. Magnesium oxide, MgO (100), and sapphire, Al_2O_3 (0001), were selected because of their favorable lattice matches to the perovskite $KNbO_3$. Using the computer-controlled ion beam sputter-deposition system developed in this program, the highest quality $KNbO_3$ thin films reported to date were grown .

The microstructures of $KNbO_3$ films grown are strongly determined by deposition temperature and substrate type. X-ray diffractometer patterns and transmission electron microscopy, TEM, have confirmed that $KNbO_3$ thin films grown on MgO at 600 °C and above are epitaxially oriented, $[110]KNbO_3//[100]MgO$, $[001]KNbO_3//[001]MgO$. Two types of defects have been observed in these films. First, tetrahedral growth twin domains, TTDs, which nucleate from steps on the MgO surface have been identified. These growth twins can be controlled by proper substrate preparation. Secondly, inversion domain boundaries, IDBs, have been found in the films in addition to the TTDs. These boundaries are charged and may affect ferroelectric switching behavior, though this has not been studied yet.

The $KNbO_3$ thin films grown on sapphire at 625 °C and above are highly oriented, $[111]_cKNbO_3//[0001]Al_2O_3$. Multiple positioning boundaries, MPBs, were observed within the (111) $KNbO_3$ films. The MPBs were categorized into three types, translational, double positioning, and translational double positioning boundaries.

3) Electro-optic characterization of $KNbO_3$ thin films.

The electro-optic effect was measured in ion beam sputter-deposited $KNbO_3$ thin films, manifested as a shift in the birefringence due to an applied electric field. Epitaxial $KNbO_3$ films on MgO (001) show a smaller birefringence shift than predicted from film geometry and bulk parameters, The discrepancy can be explained by incomplete switching of the ferroelectric domains within the films. In addition, microstructural defects were found to influence the magnitude of the birefringence shift. If poled,

however, the films may have very desirable properties for electro-optic applications.

The $KNbO_3$ thin films deposited on sapphire (0001) exhibit a large shift in the birefringence due to an applied electric field. The magnitude of this shift must be attributed to the shear components of the linear electro-optic tensor, the largest coefficients for $KNbO_3$. Due to the large birefringence shift at relatively low field levels, these films show great potential for electro-optic applications where light passes through the film plane.

4) Guided-wave characterization and device modeling.

Many integrated optics applications for electro-optic thin films require the films to serve as planar waveguides. Light was launched into the plane of ion beam sputter-deposited $KNbO_3$ thin films using the prism-coupling method to demonstrate their utility as waveguides. This method was also used to determine the index of refraction of the films by measuring the position of the coupling angles. The index of refraction for $KNbO_3$ thin films was calculated to equal 2.28, an index very near the literature values for $KNbO_3$.

To demonstrate the potential for our $KNbO_3$ thin films, a waveguide electro-optic phase modulator based on the thin films was modeled. The model optimizes the drive voltage and modulation bandwidth of the device. The epitaxial $KNbO_3$ thin films grown on MgO (001) using the ion beam sputter-deposition technique were used as the basis for the model. The characteristics of the optimized device demonstrate the potential of $KNbO_3$ films to surpass bulk single crystal $LiNbO_3$, which is currently the material of choice for guided-wave integrated optics devices.

5) Two Ph. D. theses and 15 publications resulted from the work supported by this Office of Naval Research contract no. N00014-88-K-0526.

Chapter 1

INTRODUCTION

The body of this report is composed of four reprints of papers and one chapter of a Ph. D. thesis which encompass the work performed during the tenure of the contract sponsored by the Office of Naval Research. The content of these reprints is outlined below.

The first reprint entitled "Deposition of Electrooptic Thin Films" was presented at the 92nd annual meeting of the American Ceramic Society and was published in Ceramic Transactions Vol. 14: *Electro-Optics and Non-linear Optic Materials*. The development of the ion beam sputter-deposition system is discussed along with initial microstructural studies of $KNbO_3$ thin films in this paper.

The second reprint is titled "High Resolution Imaging of Twin and Antiphase Domain Boundaries in Perovskite $KNbO_3$ Thin Films." This paper presents a detailed microstructural study of the defects found in epitaxial $KNbO_3$ thin films deposited on single crystal MgO (100) substrates. This work was presented at the Spring meeting of the Materials Research Society in 1990 and was published in the Materials Research Society Symposium Proceedings Vol. 183, *High Resolution Electron Microscopy of Defects in Materials*.

The third section is taken from the Ph. D. thesis of Shang H. Rou. Titled "Microstructural Characterization of the Epitaxial (111) $KNbO_3$ on (0001) Sapphire," this chapter describes the transmission electron microscope studies of the growth defects present in $KNbO_3$ films deposited on sapphire.

The next section is a reprint of a paper titled "Electro-optic characterization of ion beam sputter-deposited $KNbO_3$ thin films" which was published in Applied Physics Letters. The electro-optic properties of $KNbO_3$ thin films deposited on both MgO and sapphire were reported for the first time. In addition, the relationships between microstructural defects and the electro-optic properties are discussed.

The waveguiding characteristics are reported in the last section titled "Optical Characterization of Potassium Niobate Thin Film Planar Waveguides." Additionally, an electro-optic phase modulator was modeled using an ion beam sputter-deposited $KNbO_3$ thin film on MgO (001) as the basis for the model. This paper was presented at the 1991 Fall Meeting of the Materials Research Society and will be published in the Materials Research Society Symposium Proceedings, Vol. 243, *Ferroelectric Thin Films II*.

Full bibliographic listings for these reprints can be found below along with all other publications supported by the Office of Naval Research under this contract.

1.1 Theses granted resulting from work either fully or partially supported by the Office of Naval Research.

* 1. "Characterization of Perovskite Thin Films," Shang H. Rou, Ph. D. Thesis, North Carolina State University, Raleigh, NC 27695, 1990.

2. "Ion beam sputter-deposition, optical characterization, and modeling of potassium niobate thin films," Thomas M. Graettinger, Ph. D. Thesis, North Carolina State University, Raleigh, NC 27695, 1992.

1.2 Publications resulting from work either fully or partially supported by the Office of Naval Research.

* 1. "Electro-optic characterization of ion beam sputter-deposited $KNbO_3$ thin films," T. M. Graettinger, S. H. Rou, M. S. Ameen, O. Auciello, and A. I. Kingon, Appl. Phys. Lett., **58**(18), 1991, pp. 1964-1966.

2. "Ion beam sputter deposition of ferroelectric oxide thin films," T. M. Graettinger, O. Auciello, M. S. Ameen, H. N. Al-Shareef, K. Gifford, and A. I. Kingon, MRS Symposium Proceedings, Vol. 223, Low Energy Ion Beam and Plasma Modification of Materials, (MRS, Pirrsburgh, PA), 1991, pp. 273-281.

3. "Investigation of the electro-optic properties of ion beam sputter-deposited $KNbO_3$ thin films," T. M. Graettinger, S. H. Rou, M. S. Ameen, O. Auciello, and A. I. Kingon, Symposium on Ferroelectric Films, 93rd Annual Meeting of the Am. Ceramic Soc., Cincinnati, OH, May 1991.

4. "Processing-structure relations for ferroelectric thin films deposited by ion beam sputter deposition," A. Kingon, M. Ameen, O. Auciello, K. Gifford, H. Al-Shareef, T. Graettinger, S. H. Rou, and P. Hren, Ferroelectrics **116**, 1991, pp. 35-49.

* 5. "Optical characterization of potassium niobate thin film planar waveguides," T. M. Graettinger and A. I. Kingon, MRS Symposium Proceedings, Vol. 243, *Ferroelectric Thin Films II*,(MRS, Pittsburgh, PA), 1991 (in press).

6. "Microstructure and process integration of epitaxial ferroelectric thin films," S. H. Rou, T. M. Graettinger, A. F. Chow, D. J. Lichtenwalner, O. Auciello, and A.I. Kingon, MRS Symposium Proceedings, Vol. 243, *Ferroelectric Thin Films II*, (MRS, Pittsburgh, PA), 1991 (in press).

7. "Electrostatic energy induced 45° rotation in heteroepitaxial $KNbO_3$ thin films an (001) MgO," S. H. Rou, T. M. Graettinger, O. Auciello, and A. I. Kingon, MRS Symp. Proc., *Heteroepitaxy of Dissimilar Materials*, Spring 1991.

* 8. "High resolution imaging of twin and antiphase domain boundaries in perovskite KNbO3 thin films," S. H. Rou, P. D. Hren, J. J. Hren, T. M. Graettinger, M. S. Ameen, O. Auciello, and A. I. Kingon, MRS Symp. Proc., Vol. 183, *High Resolution Electron Microscopy of Defects in Materials*, (MRS, Pittsburgh, PA), 1990, pp. 285-290.

9. "Characterization of the inverted tetrahedral twin particles in the heteroepitaxial $KNbO_3$ thin films," S. H. Rou, J. J. Hren. P. D. Hren, T. M. Graettinger, M. S. Ameen, O. Auciello, and A. I. Kingon, *Proceedings of the XIIth International Congress for Electron Microscopy*, (San Francisco Press, Inc.), 1990, pp.466-467.

10. "Processing and Structural characterization of ferroelectric thin films deposited by ion beam sputtering," M. S. Ameen, T. M. Graettinger, S. H. Rou, H. N. Al-Shareef, K. D. Gifford, O. Auciello, and A. I. Kingon, MRS Symp. Proceedings, Vol. 200, 1990, pp. 65-76.

* 11. "Deposition of electrooptic thin films," A. I. Kingon, S. H. Rou, M. S. Ameen, T. M. Graettinger, K. Gifford, and O. Auciello, *Ceramic Transactions* Vol. 14, *Electro-Optics and Non-linear Optic Materials*, (Am. Cer. Soc., Westerville, OH), 1990, pp. 179-196.

12. "Computer-controlled ion beam sputter deposition of multicomponent oxides," A. I. Kingon, O. H. Auciello, M. S. Ameen, C. N. Soble, T. M. Graettinger, and S. H. Rou, *Ceramic Transactions* , Vol. 11, *Ceramic Thick and Thin Films*, (Am. Cer. Soc., Westerville, OH), 1990, pp. 47-57.

13. "Computer-controlled ion beam deposition systems for high T_c superconductor and other multi-component oxide thin films and layered structures," A. R. Krauss, O. Auciello, A. I. Kingon, M. S. Ameen, Y. L. Liu, T. Barr, T. M. Graettinger, S. H. Rou, C. N. Soble, and D. M. Gruen, Applied Surface Science, **46**, 1990, pp. 67-73.

14. "Characterization of $KNbO_3$ thin films deposited by ion beam sputtering using a computer-controlled rotating target holder," M. S. Ameen, T. M. Graettinger, O. Auciello, S. H. Rou, and A. I. Kingon, MRS Symp. Proceedings, Vol. 152, 1989, pp. 175-179.

15. "Ion beam sputter deposition of $YBa_2Cu_3O_{7-\delta}$: beam induced target changes and their effect on deposited film composition," M. S. Ameen, O. Auciello. S. H. Rou, C. N. Soble, T. M. Graettinger, A. R. Krauss, and A. I. Kingon, AIP Conf. Proc. No. 200, 1988, pp95-.

*** A reprint of the papers marked with an asterisk are included in this report.**

1.3 ACKNOWLEDGEMENTS

This research effort was carried out, for the most part, by the following research team: Dr. Michael S. Ameen (post-doctoral researcher), Dr. Shang H. Rou, Dr. Thomas M. Graettinger, and Alice F. Chow.

Useful insights from and discussions with Dr. A. R. Krauss (Argonne National Laboratory), and Dr. Nalin Parikh (UNC-Chapel Hill) are greatly appreciated.

Chapter 2

Reprinted from

"Deposition of electrooptic thin films," A. I. Kingon, S. H. Rou, M. S. Ameen, T. M. Graettinger, K. Gifford, and O. Auciell, *Ceramic Transactions* Vol. 14, *Electro-Optics and Non-linear Optic Materials*, (Am. Cer. Soc., Westerville, OH), 1990, pp. 179-196.

DEPOSITION OF ELECTROOPTIC THIN FILMS †

Angus I. Kingon*, Shang-Hsien Rou, Michael S. Ameen,
Thomas M. Graettinger, Kenneth Gifford and Orlando Auciello+
Department of Materials Science and Engineering
North Carolina State University, Raleigh, NC 27695-7907

and

Alan R. Krauss
Chemistry and Materials Science Divisions, Argonne National
Laboratory, Argonne, Illinois 60439

ABSTRACT

$KNbO_3$ thin films have been deposited on Si and MgO (100) substrates by a new ion beam sputter deposition system. It has been shown that, by choice of substrate and conditions, a variety of microstructures can be controllably achieved, varying from polycrystalline to epitaxial single crystal. In the case of the latter, two defect types have been observed, viz antiphase domains and 211-type growth twins. A structure has been postulated for the domain boundaries of the former. The relationships between microstructures and ferroelectric properties can now be investigated. Preliminary dielectric property measurements were made of polycrystalline films deposited on TiN / MgO (100) substrates. In the case of epitaxial $KNbO_3$ films on MgO substrates, light has successfully been coupled into the films, and the films show low scattering losses.

* Member, American Ceramic Society
\+ Also Microelectronics Center of North Carolina
† Invited Presentation

1. INTRODUCTION

1.1 Background to Electrooptic Thin Films

With the present trend towards developing smaller, integrated optical devices, thin film electrooptic components, such as guided wave phase modulators for optical switches, appear increasingly attractive. Electrooptic components fabricated by thin film process methods display several immediate and potential advantages, which include: processing techniques amenable to a wide range of device architectures; potentially fewer process steps and lower costs; scale of film thicknesses compatible with requirements for integrated optic devices; lower growth temperatures; (economic) tolerance for lower growth rates (thereby a potential for increased material quality); and the possibility of "graded" compositions and tailoring of refractive index profiles.

1.2 $KNbO_3$ as an Electrooptic Material

The material commonly utilized for phase modulators is $LiNbO_3$, although it does not have the highest figure of merit.[1,2] Rather, its utilization is due to its convenient fabrication in bulk single crystal form by growth from the melt. In addition, channel waveguides of cross-sectional dimensions which match optical fibers are conveniently formed by Ti ion-diffusion into the $LiNbO_3$ wafers.

Materials with higher figures of merit exist, although a precise comparison necessitates definition of the device geometry. These materials include[1,2] $KNbO_3$ (33- and 42- modes), $BaTiO_3$ (51- and 33- modes, and $Ba_2NaNb_5O_{15}$ (33- mode).

$KNbO_3$ melts incongruently, making growth of bulk, high quality single crystals difficult.[3] It has a Curie point of ~435°C, and undergoes a further tetragonal-orthorhombic transition at ~225°C.[4] The structural anisotropy promotes micro- and macrocracking during cooling through the phase transitions.

It is interesting to note that in the K_2O - Nb_2O_5 system, a number of compounds have been reported, ranging in stoichiometry from $K_6Nb_{44}O_{113}$ to $K_6Nb_2O_8$.[5] In addition, deviation from the ideal cation stoichiometry must be expected. The extent of this non-stoichiometry, of the form $K_{1-2x}NbO_{3-y}$, has not been investigated.

$KNbO_3$ is therefore a candidate thin film electrooptic material, which requires further investigation. This investigation must include the selection of suitable process methods.

1.3 Thin Film Process Methods

A number of processing methods are currently being explored for ferroelectric thin films, as discussed in an earlier paper.[6] Critical issues determining the choice include: the processing temperature limits; substrates and interfaces; defects and microstructures; and variability of composition and properties. These are briefly mentioned in turn.

Processing temperatures are determined largely by the devices required. In the case where electrooptic components need to be directly deposited on Si and GaAs semiconductors, the process temperatures are limited to typically <600°C. At these reduced temperatures the mobility of cation species is low, making the fabrication of high quality single crystal thin films difficult.

The choice of substrate is determined by the device architecture, the required refractive index mismatch, and the lattice match between substrate and film (if epitaxial films are required). Direct deposition on Si and GaAs presents the problem of the lattice mismatch with $KNbO_3$, and the formation of amorphous oxide layers at the interface.

For most electrooptic applications, it is likely that epitaxial single crystal films will be required, as grain boundaries in polycrystalline films can act as scattering centers, and as a source of defects. This postulate has yet to be confirmed. Lattice defects can yield optical centers and photocarriers, with the resultant transient currents being detrimental to the electrooptic device performance. Unfortunately, detailed relationships between lattice defects and properties, and more generally between microstructures and properties, have not been established for these materials. This must remain a topic of research.

The variability of properties from sample-to-sample and batch-to-batch is an issue central to commercialization of these materials. Tight constraints are imposed on processing, with the control of cation stoichiometry a well-identified problem.

The two techniques most commonly utilized for the deposition of electrooptic and other ferroelectric films are sol-gel processing (or a variant thereof), and magnetron sputtering. While both techniques

possess a set of valuable advantages, it is important to be aware of their respective disadvantages.

Sol-gel films usually utilize spin-on deposition of organometallic precursors, with film thicknesses $\geq 0.3\ \mu m$ requiring multiple depositions. Problems normally encountered are film cracking and porosity, which can be attributed to large volume changes upon drying, or upon pyrolysis and loss of the organic component. The process makes nucleation and growth of the crystalline films difficult to control in comparison with a vapor deposition process, and thus there is difficulty in producing epitaxial films at comparably low temperatures.

Magnetron (or plasma) sputtering has as a major disadvantage in the fact that the plasma interacts directly with the growing film. In the case of oxide deposition, this results in the so-called "negative ion effect"[7], as well as electron bombardment [8], and inert gas incorporation. Methods which minimize the negative ion effect [9], inevitably have a large negative influence on the film growth rate.

In addition, it is common in plasma sputtering to use single multicomponent oxide targets. The problem of stoichiometry control in the presence of preferential sputtering effects has been documented previously.[10] While these effects can be minimized in the short term, the prognosis for commercial-scale processes must be carefully weighed.

Because of the disadvantages mentioned above, new processing methods for multicomponent oxides are presently being explored. In this paper we describe the application of a computer-controlled ion beam sputter deposition technique to $KNbO_3$ thin films, and demonstrate the extent to which microstructures may be controlled.

2. EXPERIMENTAL

2.1 Computer Controlled Ion Beam Sputter Deposition

The system is shown in Figure 1. The deposition system consists of a Nb-lined stainless steel chamber turbopumped to a base pressure of about 1.0×10^{-7} torr, an Ar^+ ion beam of 1.4 keV and 25 mA, and a quartz lamp heater assembly capable of heating the substrate to > 600°C. The system geometry shown in Figure 1 was chosen based on previous studies performed on Ar^+ backscattering and incorporation into

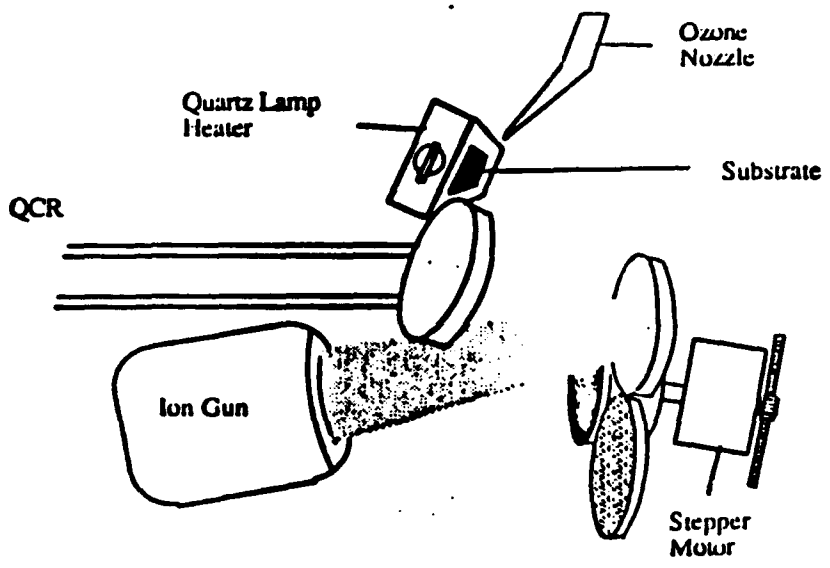

Fig. 1. Schematic of the computer controlled ion beam sputter deposition system.

the growing film.[11,12] These studies indicate that, for Ar^+ ions, near normal beam incidence on the target with the substrate positioned close to the beam axis results in a minimization of ion scattering from the target and thus of gas incorporation into the growing film. Further reduction of deleterious ion scattering effects can be achieved by using source ions of higher atomic mass, such as Kr^+ and Xe^+.[11,12] The quartz crystal resonator (QCR) and substrate are positioned symmetrically about the beam-target (mirror) plane to ensure accurate measurement of the sputtered flux.

A typical deposition cycle proceeds in the following manner: After sputtering from a target, the computer turns the ion beam off, then activates the stepper motor, which rotates a new target into position in front of the ion beam. Switching the beam off in this manner minimizes possible contamination of the film that may arise from sputtering of the holder material during the transition from one target to another. As a

precaution the holder is constructed of niobium. The QCR is then automatically programmed by the computer to the density value of the next target material, the thickness reading is reset to zero, and the ion beam is switched on to sputter the target. The thickness of the layer is monitored until the programmed set point is reached. This is presently done with less than 1% variation in layer thicknesses. Typical layer thicknesses are 1 - 20Å at the substrate. The cycle is repeated with each component until the desired film thickness is obtained. [Further details related to this novel method will be published elsewhere.][13]

2.2 Deposition of $KNbO_3$

Using the technique described above, $KNbO_3$ films have been deposited onto either (100) Si or (100) MgO single crystal substrates. Some samples were deposited on TiN films which had in turn been deposited on the MgO substrates. The MgO was chemically cleaned and annealed to remove surface damage. Targets, constructed from KO_2 pressed in a N_2 atmosphere and Nb metal, were fitted into Nb retaining rings and installed on the rotating platen shown in Figure 1. The substrates were heated to between 450°C and 600°C during deposition, and cooled slowly to room temperature.

For the films reported in this study, computer set points for the individual layer thicknesses were 10Å for the Nb and 20Å for each of the two KO_2 targets. These layers interdiffuse at the elevated substrate temperatures to yield $KNbO_3$ in situ. Investigations on reduced layer thicknesses are currently underway. Depositions consisted of approximately 75 rotation cycles, yielding films about 1500Å in thickness. It is assumed that the deposited potassium species is K_2O. Films were transparent with a very slight yellow coloration (typical of $KNbO_3$ single crystals).

2.3 Film Characterization

Films were characterized by x-ray diffraction using Cu Kα radiation, and by cross-sectional and plan view transmission electron microscopy using a Hitachi H800. High resolution electron microscopy was performed on a JEOL 200CX. Special TEM specimen preparation procedures have been developed, which will be reported elsewhere.[14]

For samples deposited on TiN / Mgo substrates, impedance was measured over the frequency range 5-1000 kHz using a Hewlett-Packard 4192A impedance analyzer.

$KNbO_3$ was deposited on Si (100), MgO (100) and TiN / MgO (100) substrates at substrate temperatures in the range 450 - 600°C.

3. RESULTS AND DISCUSSION

Over a small range of K:Nb ratios, the desired single phase perovskite $KNbO_3$ resulted. Excess K_2O appeared to be evaporated, with the surface morphology showing some dependence upon this K_2O excess.

Despite varying the K:Nb ratio over a wide range, the only other phase detected was KNb_3O_8. This is in marked contrast to the reported phase diagram which was determined using K_2CO_3, in the presence of atmospheric water vapor.[5] Noting the absence of atmosphere in the present vacuum system and the short interdiffusion distances required for reaction, it is deduced that a number of the previously reported phases are stabilized by H_2O and / or CO_2.

A major objective of the present work was to determine the range of microstructures which could be achieved. Table 1 summarizes the results for Si and MgO substrates.

Table 1 Summary of $KNbO_3$ Microstructures Observed

Substrate	Substrate Temperature (°C)	Microstructures	Figures numbers
Si	500	amorphous	
	550	microcrystalline, amorph. matrix	
	600	polycryst., little orientation	2
MgO	500	amorphous	
	550	mixture non-oriented and epitaxial	3
	600	epitaxial,mostly single crystal	4,6,7
TiN/MgO	600	polycrystalline	

Selected microstructures are shown in Figures 2-7. Figure 2 is a cross-sectional TEM micrograph of $KNbO_3$ deposited on Si (100) at 600°C. It is apparent that there is a significant formation of amorphous SiO_2 at the interface. EDS analysis showed no measurable concentration of potassium in this interface layer. The polycrystallinity is an expected result of the amorphous interface. Analysis of further samples indicates that the thickness of the amorphous SiO_2 layer is variable, and dependent upon process conditions. The surface roughness of the $KNbO_3$ films on silicon is a function of the grain size, and which is is ~ 0.5 - 1.0 μm at 600°C deposition temperature.

Figure 3 shows a plan view TEM micrograph of $KNbO_3$ deposited on MgO (100) at 550°C. The film is polycrystalline, with some grains displaying an orientational relationship (dark grains) to the substrate, and with others showing no apparent correlation. This result is confirmed by x-ray diffraction. It is interesting to note that at the same deposition temperature, films on Si are predominantly amorphous, with some randomly aligned microcrystalline regions, about 20 - 30 nm in diameter. This emphasizes the role of the substrate on the nucleation and growth process.

Figures 4, 6 and 7 show microstructures of $KNbO_3$ deposited on MgO (100) single crystal substrates at 600°C. X-ray diffraction and selected area electron diffraction indicate that the whole film has an epitaxial relationship to the substrate.

The film appears to have tetragonal symmetry, rather than orthorhombic. Selected area diffraction (SAD) of cross-sectional TEM samples indicates that the c-axis is oriented perpendicular to the plane of the film. It should be emphasized that the film is epitaxial to the substrate, and not simply oriented, as the a and b axes of the film match directly onto the a and b axes of the cubic MgO substrate. Figure 4 shows a high resolution lattice image of a film in plan view. The measured interplanar spacings confirm the lattice parameters of a (=b) = 4.0 ± 0.05 Å . High resolution images also indicate that there are two types of defect types present in these single crystal films, viz antiphase domain boundaries (APDs) and growth twins. The antiphase domain boundaries represent stacking faults in the cation sublattice, i.e., a transposition of A and B sites across the bound and a shift of one half of a unit cell. An APD has been outlined in Fig. 4. The boundary encloses a volume element. The concentration of these APDs varies

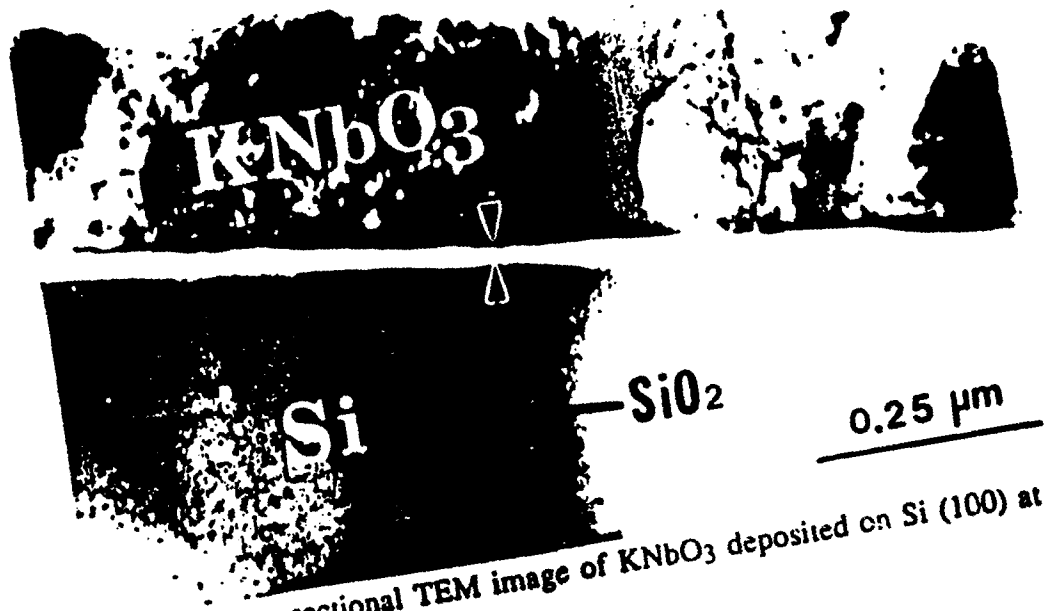

Fig. 2. Cross-sectional TEM image of $KNbO_3$ deposited on Si (100) at 600°C.

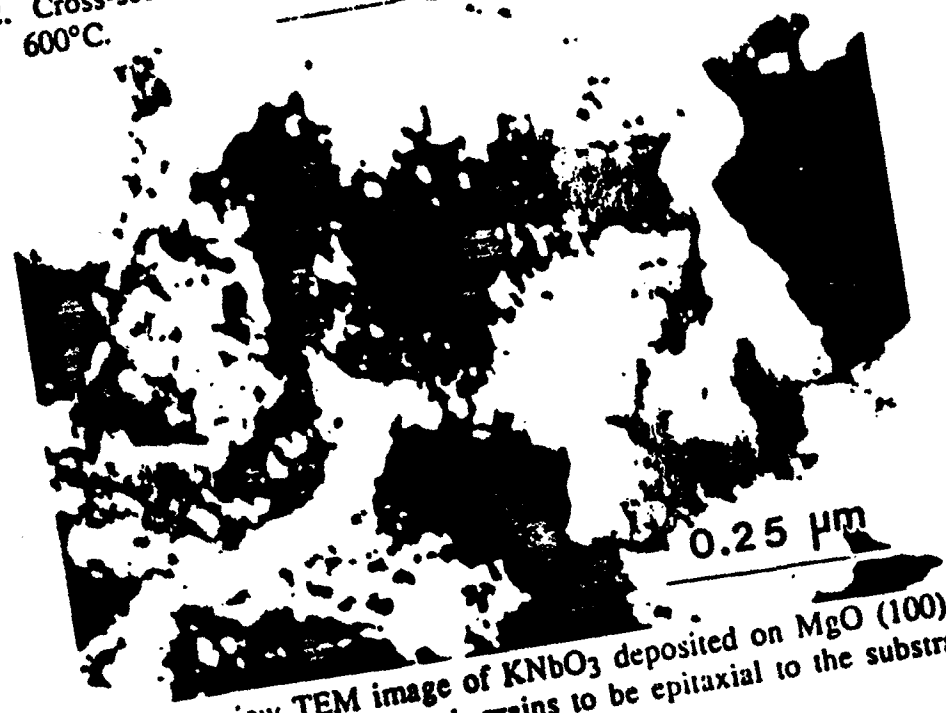

Fig. 3. Plan view TEM image of $KNbO_3$ deposited on MgO (100) at 550°C. SAD indicates the dark grains to be epitaxial to the substrate.

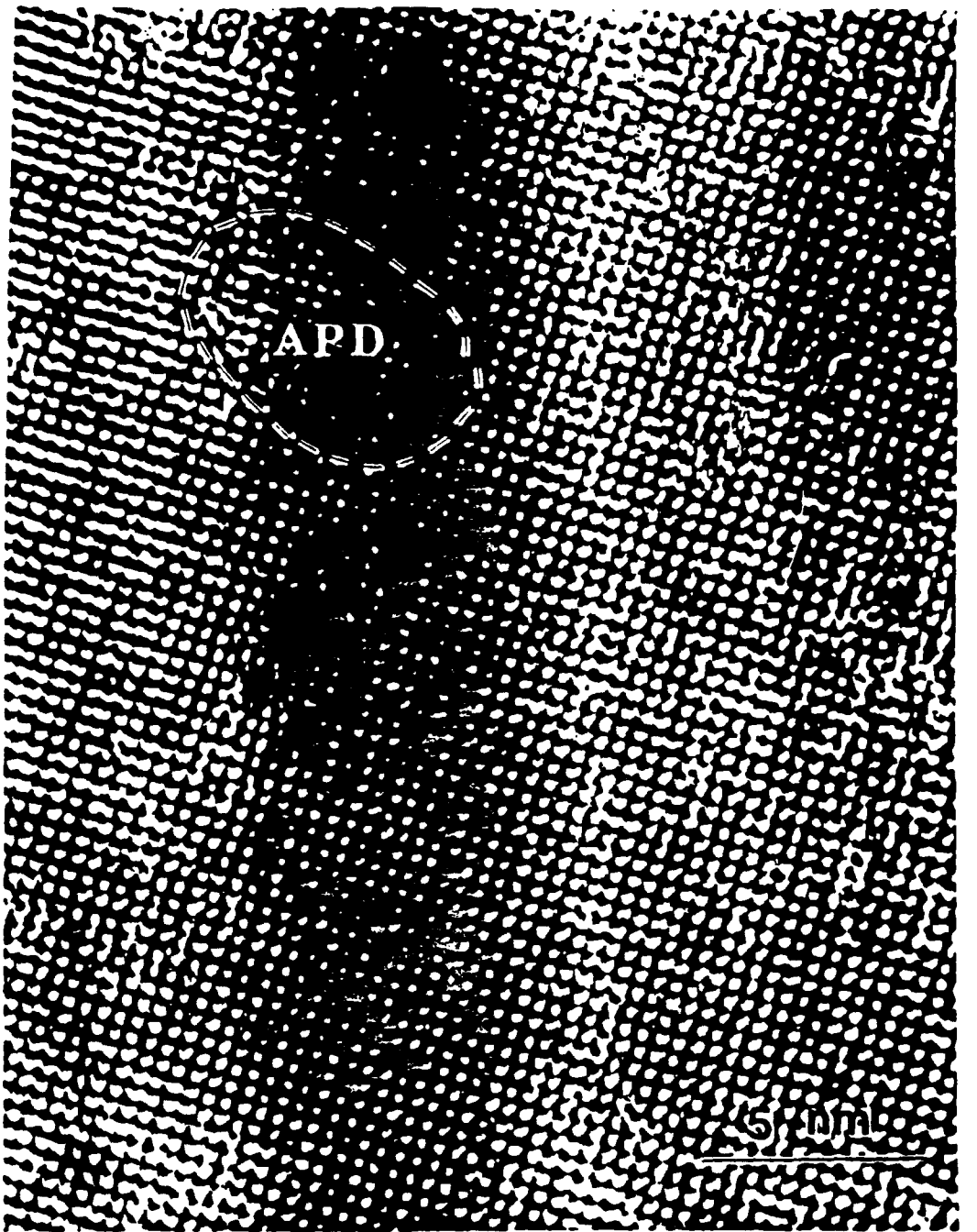

Fig. 4. High resolution electron microscope image of epitaxial $KNbO_3$ on a MgO (100) substrate. An APD is outlined.

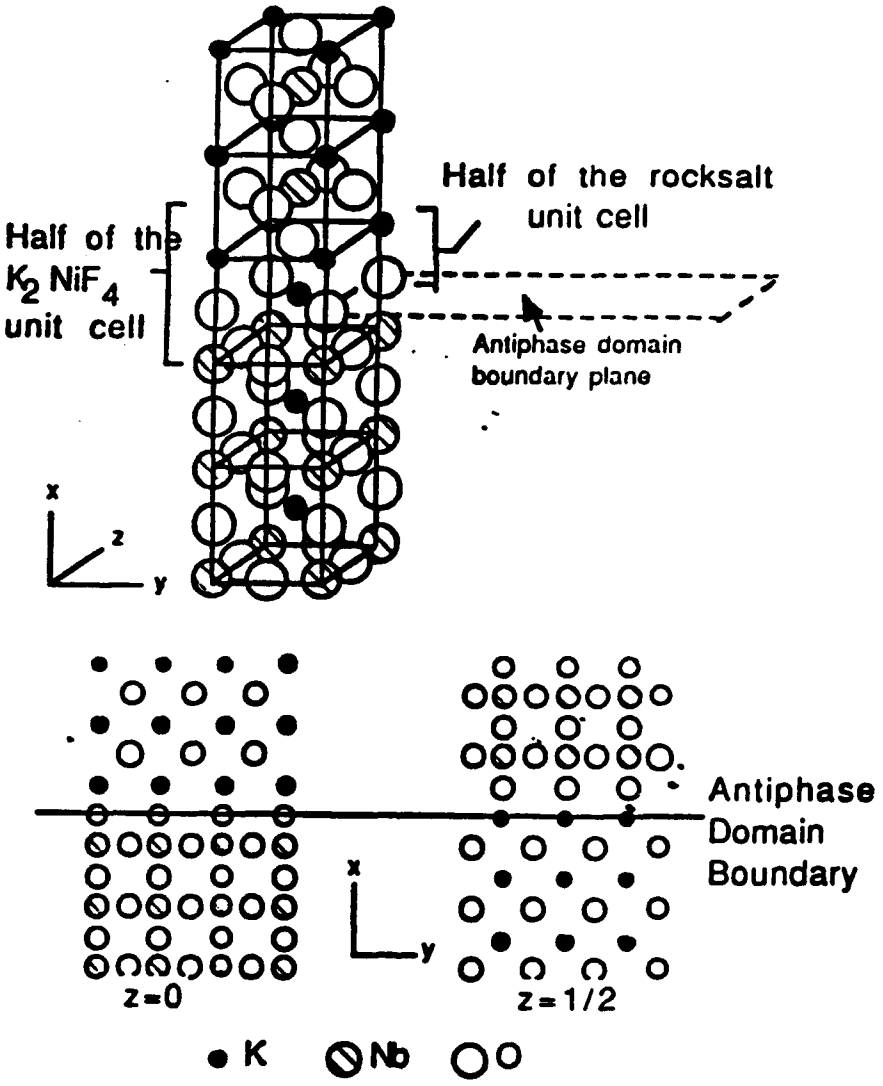

Fig. 5. Postulated structure of the antiphase domain boundary (APD).

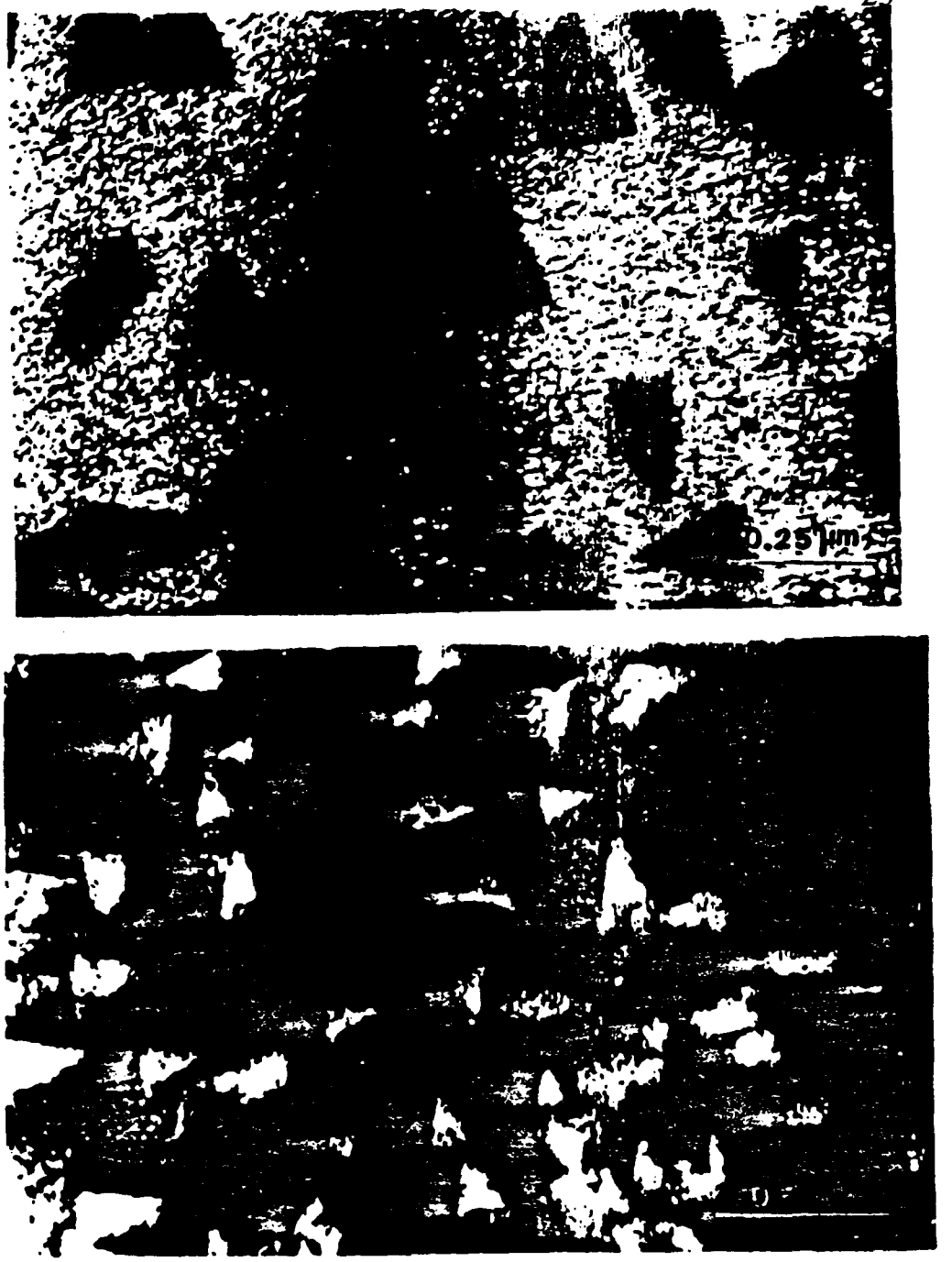

Fig. 6. Plan view images of a heteroepitaxial $KNbO_3$ film showing the 211-type growth twins.

both within one film, and from film-to-film. The origin of the stacking faults could either be due to nucleation of growth at various points within the film, or (if nucleation occurs at the interface as is desired), then due to steps and ledges on the MgO substrate surface.

A postulated structure for the boundary is shown in Figure 5. This postulated structure is expected to be of low free energy. The niobium retains coordination to six oxygens in an octahedral site, while the structural inversion occurs around potassium, with four of its adjacent oxygens in "next nearest neighbor" sites being replaced by a single oxygen in a "nearest neighbor site". This is considered acceptable for the more ionic bonds to the A-site K^+ cation, as a local rocksalt-type structure results right at the boundary. The postulate that this is a low energy boundary is strengthened by the fact that the structure emulates half the unit cell of the K_2NiF_4 structure, which is a common variant of the perovskite structure.[15] However, it should be noted that this postulated structure is less favourable for $A^{1+}B^{5+}O_3$ perovskites. This is due to the fact that in the case of the former, there is a net charge associated with each plane of the {200} type, alternating in sign, for a net zero charge. In the case of $A^{2+}B^{4+}O_3$ perovskites, each plane is a zero net charge. Therefore, introduction of a APD as shown in Fig. 5 results in a disruption in the alternating charges in $KNbO_3$, making it significantly less favourable than for the case of $A^{2+}B^{4+}O_3$ structures. The method of compensating for the excess charge at the APD boundary is $KNbO_3$ is not known, but is presumably by oxygen vacancies. Computer simulations of the possible structures, including that shown in Fig. 5, are presently being undertaken.

The other type of defect observed is a growth twin. This is being reported in more detail elsewhere.[16] Figures 6a and 6b are plan view images of these twins. These growth twins have twin boundaries of the {211} type. The twins are therefore of inverted tetrahedral shape, with the triangular base having angles of 71, 71 and 38°. The twins can be pointed in one of four orthogonal directions. A portion of a twin, the "point", is shown in a plan view high resolution atomic image in Fig. 7. The boundary is curved rather than being "sharp" down to atomic dimensions in order to maintain charge stoichiometry.

In the case of these growth twins, it should be noted that the allowed directions of the polarization vectors differ from those of the matrix. This will affect the overall dielectric displacement. The effect on domain wall mobility and thus on switching processes, has not been established.

Initial characterization of the dielectric properties of the films deposited on TiN / MgO has been undertaken. Measurements were made between silver electrodes sputter deposited on the top surface, and the TiN electrode at the $KNbO_3$ lower surface. These particular films were polycrystalline. (Details will be reported elsewhere.[17]) No dielectric breakdown was observed at the maximum applied fields of 1×10^8 Vm^{-1} (1000 kV per cm). The relative dielectric constant decreased from ~100 to ~55 over the frequency range 1 kHz to 1 MHz. However, films were lossy, with tan σ about 0.1. Although the TiN electrode contained some oxygen, no insulating interface (for example $MgTiO_4$ or TiO_2) was observed at the TiN - $KNbO_3$ interface.[17]

In the case of the epitaxial films deposited directly onto MgO substrates, the coupling of light directly into the film was achieved. The configuration is shown schematically in Figure 8. For thicker films (~0.5 μm), up to four coupling modes were observed. Relatively little scattering occurs in the film. The analysis of the coupling modes is presently being undertaken, and will be extended to direct measurement of in-plane transmission losses and electrooptic coefficients.

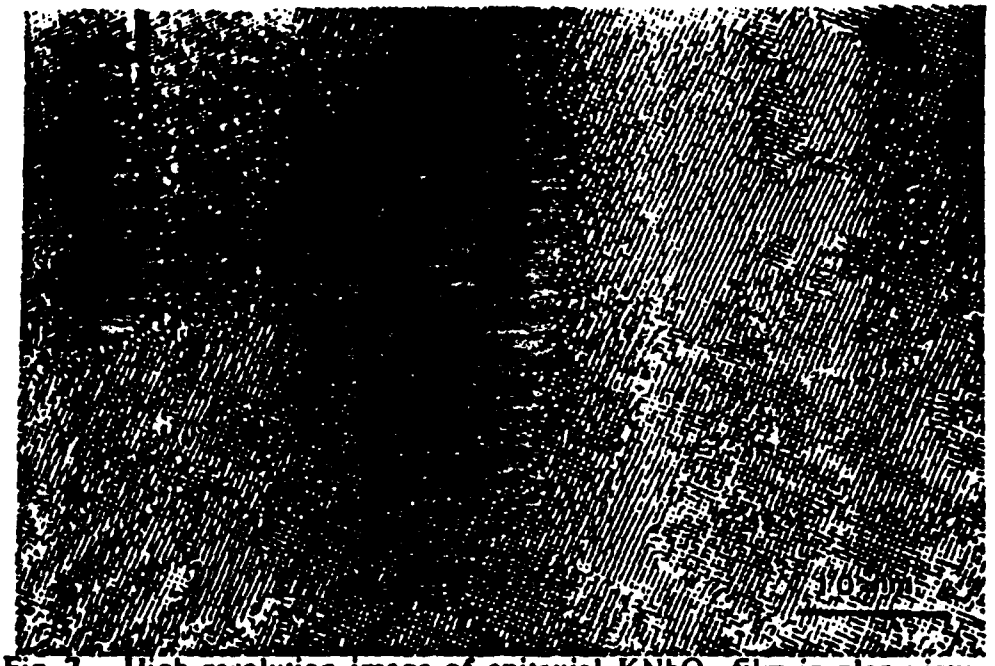

Fig. 7. High resolution image of epitaxial $KNbO_3$ film in plan view, showing "point" of growth twin of the type seen in Figs. 6a and 6b.

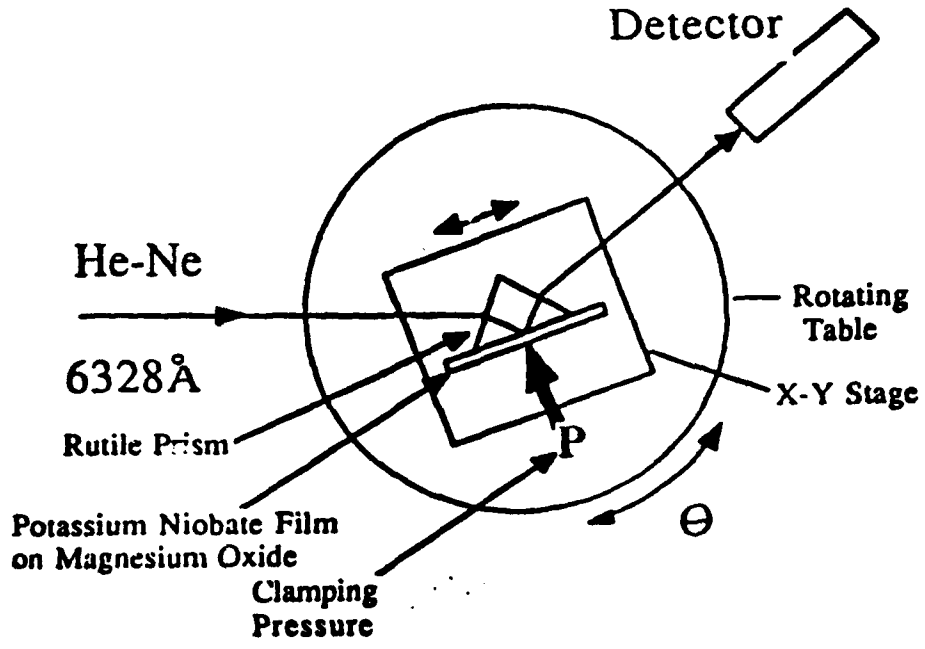

Fig. 8. Schematic of the method for coupling light from a laser source into the plane of the film.

4. CONCLUSIONS

The conclusions of this work may be summarized as:

a) A new computer-controlled ion beam sputter deposition technique has been applied successfully to the synthesis of $KNbO_3$ thin films.
b) Phases observed are $KNbO_3$ and KNb_3O_8, significantly fewer than previously reported in a study of the K_2CO_3 - Nb_2O_5 phase diagram.
c) A variety of microstructures can be controllably produced in $KNbO_3$ films, ranging from fine-grained polycrystalline to epitaxial single crystal.
d) Polycrystalline films can be produced on Si (100) substrates, with an amorphous SiO_2 interface layer always observed.
e) Heteroepitaxial single crystal films can be deposited on MgO (100) substrates at 600°C.
f) Two types of defects can be observed in the epitaxial films, viz antiphase domain boundaries and {211} growth twins. The effect of these defects on properties have not been determined definitively.
g) The epitaxial films appear to have tetragonal symmetry at room temperature, rather than the expected orthorhombic symmetry.

h) Preliminary dielectric measurements have been performed on polycrystalline films on TiN /MgO substrates.
j) A laser beam (λ = 633 nm) has been coupled into epitaxial films on MgO substrates. Several modes or overtones have been observed. Scattering losses are low.
k) Microstructure-property relationships are presently being determined.

ACKNOWLEDGMENTS

The authors would like to thank Drs. P.D. Hren, J.H. Hren, D. Maher, K. Bachmann and R.F. Davis for useful discussions.

This work is supported by the Office of Naval Research under Contract N00014-88-K-0526, while partial support is provided by the Defense Advanced Research Projects Agency, the National Science Foundation and the Department of Energy (A.R.K).

REFERENCES

1. R.L.Holman, L.M.A. Johnson, D.P. Skinner, "The Desirability of Electrooptic Ferroelectric Materials for Guided Wave Optics," In Proceedings of the 6th IEEE Int. Symp on the Appl. of Ferroelectrics, p. 32-40, IEEE New York, 1986.

2. B.A. Tuttle, "Electronic Ceramic Thin Films, Trends in Research and Development," *MRS Bulletin*, Oct/Nov, 40(1987).

3. E.T. Wu, J.J. Ratto, J.R. Oliver, and RR. Neurogaonker, "Growth and Properties of Ferroelectric $KNbO_3$ Single Crystals," In Proceedings of the 6th IEEE Int. Symp on the Appl. of Ferroelectrics, p. 478-81, IEEE New York, 1986.

4. Landolt-Börnstein, Numerical Data and Functional Relationships in Science and Technology, New Series, Vol 16a, Eds. T. Mitsui and S. Nomura, pgs. 48-52, Springer-Verlag, Berlin, 1981.

5. A. Reisman, "Phase Equilibria in the System K_2CO_3 - Nb_2O_5 by the Method of Differential Thermal Analysis," Soc. 77, 2115 (1955).

6. A.I. Kingon, O.H. Auciello, M.S. Ameen, C.N. Soble, T. Graettinger, S.H. Rou and A.R. Krauss, "Computer-Controlled Ion Beam Sputter Deposition of Multicomponent Oxides," accepted for publication in the Proceedings of the Symposium on Ceramic Thick and Thin Films, Indianapolis, April 1989.

7. S.M. Rossnagel and J.J. Cuomo, "Negative Ion Effects During Magnetron and Ion Beam Sputtering of $YBa_2Cu_3O_7$," Eds. J.M.E. Harper, R.J. Colton and L.C. Feldman, Amer. Inst. of Phys Conf. Proc. No. 165, 106-113 (1988).

8. N. Terada et al, "Sputter Synthesis of YBa_2Cu_3Oy As-Deposited Superconducting Thin Films from Stoichiometric Targets: A Mechanism of Compositional Deviation and its Control," Jap. J. of Appl. Phys. 27, L639-42 (1988).

9. O. Auciello, A.R. Krauss, A.I. Kingon and M.S. Ameen, "A Critical Analysis of Techniques and Basic Phenomena Related to Deposition of High Temperature Superconducting Thin Films," accepted for publication in SEM Int.

10. O. Auciello, M.S. Ameen, T.M. Graettinger, S.H. Rou and A.I. Kingon, "Ion Beam Sputter Deposited $YBa_2Cu_3O7-\sigma$: Beam Induced Target Changes and their Effect on Deposited Film Composition," accepted for publication in the Amer. Inst. of Phys. Conf. Proc. (AVS Annual Meeting, Atlanta, Oct. 1988).

11. M.S. Ameen, O. Auciello, A.R. Krauss, A.I. Kingon and M.A. Ray, "Studies on Ion Scattering and Sputtering Processes in Ion Beam Sputter Deposition of High Temperature Superconducting Films," published in AIP Conf. Proceedings, 182, 61 (1989).

12. M.S. Ameen, O. Auciello, A.R. Krauss and A.I. Kingon, "Studies on Ion Scattering and Sputtering Processes Relevant to Ion Beam Sputter Deposition of Multicomponent Thin films," submitted to the Proc. of the Mat. Res. Soc. Fall Meeting, Boston, Nov. 1989.

13. A.R. Krauss, O. Auciello, A.I. Kingon, M.S. Ameen, T. Barr and Y.L. Liu, "A Novel Computer Controlled Ion Beam Sputter Deposition System," submitted to Rev. Sci Instr.

14. S.H. Rou, P.D. Hren and A.I. Kingon, "Preparation of Cross-sectional and Plan View TEM Samples of Thin Films on MgO Substrates with an Additional Chemical Thinning Step," to be presented at the Mat. Res. Soc. Spring Meeting, San Francisco, April 1990.

15. F.S. Galasso, "Structure and Properties of Inorganic Solids," p.189, Pergamon Press, Oxford (1970).

16. S.H. Rou, P.D. Hren, T.M. Graettinger, M.S. Ameen, O.H. Auciello and A.I. Kingon, "High Resolution Imaging of Twin and Antiphase Domain Boundaries in Perovskite $KNbO_3$ Thin Films," to be presented at the Mat. Res.Soc. Spring Meeting, San Francisco, April 1990.

17. A.I. Kingon, S.H. Rou, P.D. Hren, M.S. Ameen, T.M. Graettinger, K. Gifford and O. Auciello, "Microstructure-Property Relationships for Ferroelectric Thin Films Deposited by Ion Beam Sputtering, to be submitted to the IEEE Transactions on Ultrasonics, Feroelectrics and Frequency Control (Special Issue on Ferroelectric Thin Films) To be published May 1990.

Chapter 3

reprinted from

"High resolution imaging of twin and antiphase domain boundaries in perovskite KNbO3 thin films," S. H. Rou, P. D. Hren, J. J. Hren, T. M. Graettinger, M. S. Ameen, O. Auciello, and A. I. Kingon, MRS Symp. Proc., Vol. 183, *High Resolution Electron Microscopy of Defects in Materials*, (MRS, Pittsburgh, PA), 1990, pp. 285-290.

31

HIGH RESOLUTION IMAGING OF TWIN AND ANTIPHASE DOMAIN BOUNDARIES IN PEROVSKITE $KNbO_3$ THIN FILMS.

Shang H. Rou , Philip D. Hren, John J. Hren, Thomas M. Graettinger, Michael S. Ameen, Orlando H. Auciello**, and Angus I. Kingon
Department of Materials Science and Engineering, N. C. State University, Raleigh, NC.

**Also, Microelectronics Center of N. C., Research Triangle Park, NC.

ABSTRACT

Perovskite $KNbO_3$ thin films were heteroepitaxially deposited onto (100) MgO substrates. Twin domains with tetrahedral shape were typically observed. These tetrahedrons were bounded by three {211} twin planes. High resolution transmission electron microscopy (HRTEM) was employed to examine these {211} twin boundaries. Surface steps of {110}<110> type generated by dislocation slip were present on the MgO substrate. The tetrahedral twin domains originate on surface steps, then grow with a stacking fault relationship to the matrix. The strain fields of dislocations near the stacking faults slightly rotate the tetrahedral twin nuclei. This small degree of misalignment between the matrix and the twin domain result in some of the twin boundaries having amorphous boundary regions rather than coherent interfaces.

Order-disorder antiphase domains (APD's) were directly imaged with HRTEM. Ultra small APD's ranging from 10 to 30 atomic spacings were observed. The origin of these APD's was either the surface steps of {100}<110> type on MgO substrates or the random nucleation of anions at either of two equivalent sites on the MgO substrate.

INTRODUCTION

Perovskite $KNbO_3$ has a pseudocubic structure with lattice parameters a=b=4.03Å, c=3.9739Å, α=89.7°, and $\beta=\gamma$=90° at room temperature [1]. Epitaxial $KNbO_3$ thin films were deposited onto (100) MgO substrate. We observed two types of defects, namely tetrahedral twin domains (TTD's) and antiphase domains (APD's), in the heteroepitaxial $KNbO_3$ thin films. The orientation difference between the TTD's and the matrix may affect the polarization switching process. The APD boundaries may act as light scattering centers and/or ferroelectric domain wall pinning sites. It is essential to understand the origin of these two types of defects and eliminate them if possible. HRTEM was employed to investigate the boundary structure of these two types of defects.

EXPERIMENTAL PROCEDURE

Epitaxial thin films of $KNbO_3$ were deposited onto (100) MgO substrates at 600°C with an unique computer-controlled rotating-target ion beam sputtering technique [2]. Plan view TEM samples were prepared by the usual procedure plus an additional hot orthophosphoric acid thinning step after dimpling. The specimens were subsequently ion milled in a liquid nitrogen cold stage using 4 KeV Ar^+ ions at a total gun current of 0.5 mA for a few minutes (depending on the thickness of the films) to obtain an ultrathin area for HRTEM examinations. Details of sample preparation procedure are presented elsewhere [3]. High resolution microscopy was performed on a JEOL 200CX TEM at 200 KeV.

Mat. Res. Soc. Symp. Proc. Vol. 183. © 1990 Materials Research Society

RESULTS AND DISCUSSION

Figure 1a shows a dark field microstructure of the $KNbO_3$ thin films. Four sets of triangular domains embedded in the matrix with a 90° rotation to each other were observed in this microstructure. The orientation relationships between the TTD's and the matrix are $[001]_{matrix} // [221]_{TTD}$. A schematic drawing of four sets of TTD's viewed from the (001) $KNbO_3$ matrix is shown in figure 1b. Three {211} interfaces which bounded the TTD's are indexed in figure 1b. Structure and microstructure characterization of the TTD's using conventional TEM will be presented elsewhere [4]. Surface steps of {110}<110> on MgO substrate are the origin of four sets of TTD's [4].

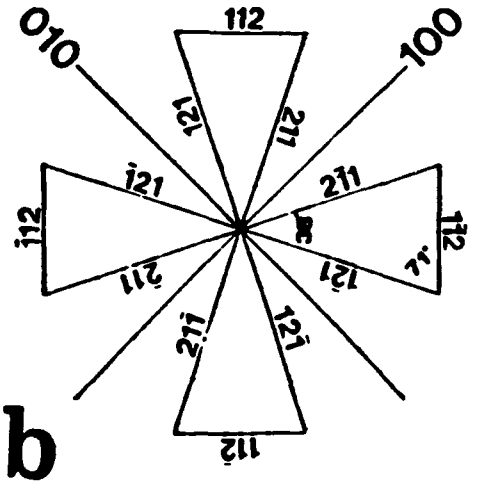

Figure 1. (a) Dark field micrograph of $KNbO_3$ thin film showing four sets of 90° rotated TTD's embedded in the (001) $KNbO_3$ matrix as indicated by arrows. (b) Schematic drawing of four sets of TTD's viewed along (001) $KNbO_3$

A high resolution electron micrograph of the $KNbO_3$ thin film taken along (100) matrix in the vicinity of a TTD is shown in figure 2. This high resolution image with a point to point resolution of ~3Å was observed in the matrix region. Lattice fringes with an interplanar spacing of ~2.84Å corresponding to {110} planes were resolved within the twin domain. The image in the matrix regions is constructed by crossed fringes of {100} and {010}. The high resolution image within the twin domain are formed by crossed fringes of {110} and {120}. Because the d-spacing of {120} is ~1.79Å which exceeds the resolution limit of the microscope, only lattice fringes are observed. Figure 3 illustrates the atomic configuration of a (221) TTD embedded in the (001) matrix. By comparing the atomic configuration with the HRTEM image, we deduce the region shown in figure 2 is near a "point" of a TTD. In addition, two twin planes which bounded this twin region were (112) and (121). Thus, the theoretical interception angle is 71°. This angle is rounded off. The local charge balance is minimized with this geometric configuration. Figure 2 also reveals that some regions near the twin interfaces show overlapping of the (100) crossed fringes and the (110) lattice fringes. This suggests that the twin interfaces are inclined with respect to the electron beam direction. The coherency interfaces between the twin domain and the matrix were evidenced by matching the {110} across the twin boundaries.

An amorphous region is found along the twin interface as shown in figure 2. This incoherent twin boundary can be attributed to the slight misorientation between the TTD and the matrix. It is believed that this slight misorientation is induced by dislocations on the MgO substrate surface. The strain field around the dislocations may slightly alter the orientation of the nuclei and, then, causes the misorientation between TTD's and matrix. Since the TTD's are inverted [4], the misorientation, which generates stress concentration

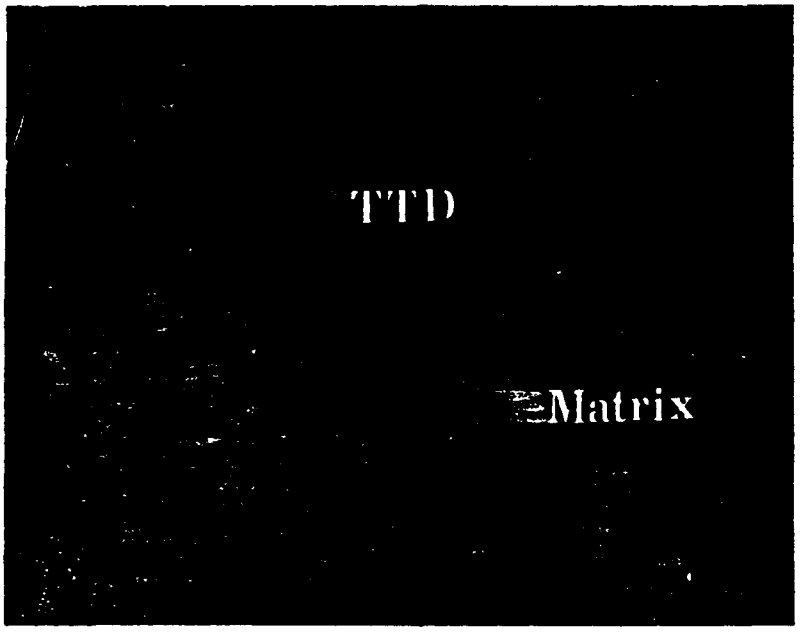

Figure 2. HRTEM micrograph of the region near a "point" of a TTD. This region is bounded by (112) and (121) twin interfaces. Amorphization region was observed along the (112) twin interface as indicated by the arrow "a". Inclined twin boundaries is indicated by arrow "b".

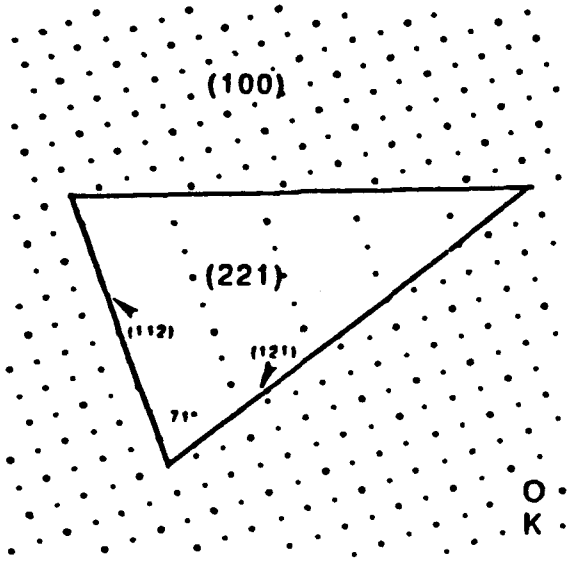

Figure 3. Atomic configuration of a TTD embedded in (100) $KNbO_3$ matrix.

along the twin interfaces, is accommodated by the lattice when the TTD is small. As the thickness of the thin film increases, the area of the TTD becomes larger. Therefore, stress concentration along the twin interfaces builds up. Once the stress concentration exceeds the critical limit, boundary amorphization occurs.

The misorientation angle of 2° to 4° is obtained by measuring the angle between the (110) TTD and the (110) matrix in figure 2. It is interesting to note that the amorphous region is only observed along the (112) interface while the (211) and (121) interfaces are coherent. The cause of this amorphous region along this particular twin interface is not yet clear. However, the misorientation between the TTP and the matrix induces stress concentration along three twin interfaces. The stress relaxation mechanisms along three {211} twin interfaces are different because the atomic configuration between the TTP and the matrix across (112) twin interface is different from those across (211) and (121) twin interfaces (figure 3). The stress concentration results in separation of the (112) interface. The amorphous region along this (112) twin interface is formed to accommodate the stress concentration. Where the stress can be accommodated by gradual lattice distortion across the (121) and (211) twin interfaces. Therefore, the coherency along these twin interfaces are maintained.

Figure 4 shows a high resolution electron micrograph of the $KNbO_3$ thin films. Small domains, ranging from 10 to 30 atomic spacings, are observed in this micrograph. Each adjacent domain shows a half lattice spacing shift with respect to each other. This domain structure is similar to the antiphase domain (APD) reported in $AuCu_3$ materials [5]. The APD's in the $KNbO_3$ thin films are the result of random nucleation of $KNbO_3$ nuclei at either of two equivalent sites or the surface steps of a/2 {100}<110> type on MgO substrates. Because of the small size of the APD's, we surmise that the density of the nuclei has to be very high. Attempts to eliminate these APD's by varying processing procedures are currently underway. Preliminary results indicate that the density of APD's is heavily dependent on the defect density on the substrate surface

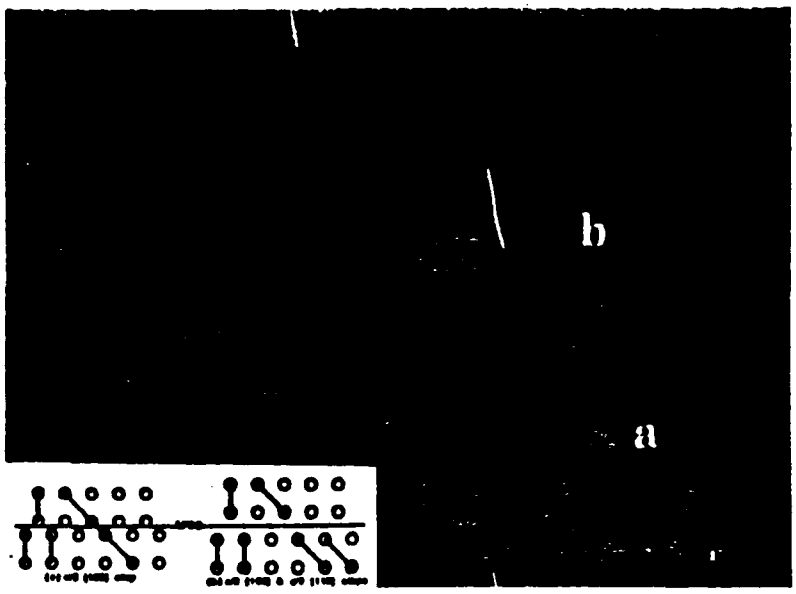

Figure 4. A typical high resolution microstructure of $KNbO_3$ thin film showing a high density of APD's. (APDB "a" shows an a/2<100> step and "b" shows an a/2<100> & a/2<110> step). The insertion is a sketch of APDB "a" and "b".

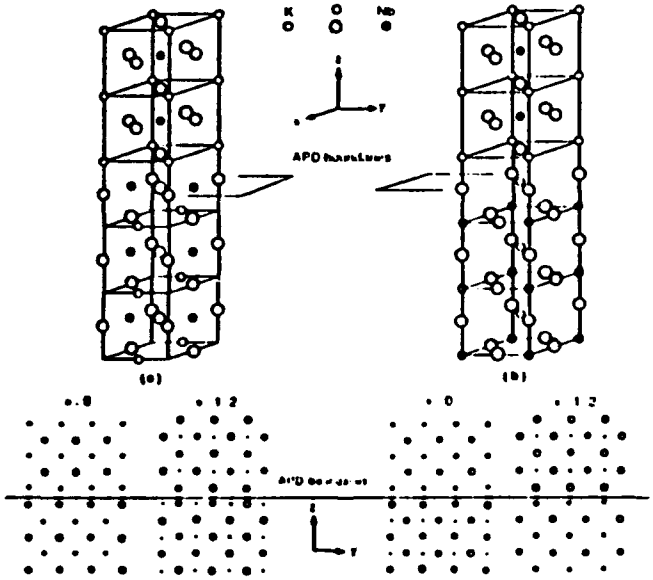

Figure 5. Atomic models of APD's. (a) a/2<100> and (b) a/2<111> translations.

The APD's structure can be built up geometrically by translation of two adjacent domains by either a/2<100>, a/2<110>, or a/2<111> with respect to each other. With these three types of lattice translations, eight possible APD boundaries with two types of structure steps, i.e. a/2<100> and a/2<100> plus a/2<110>, result. The insertion in figure 4 shows the sketch of these two types of steps. Figure 5 shows two representative atomic configurations of the APD boundary structures. The APD boundary structure shown in figure 5a is obtained with a lattice translation of a/2<100> of the bottom half of the lattice with respect to the top half of the lattice, while a lattice translation of a/2<111> leads to the APD boundary structure shown in figure 5b.

CONCLUSIONS

Thin film $KNbO_3$ was heteroepitaxially deposited onto a (100) MgO substrate. TTD's and APD's were observed in the heteroepitaxial $KNbO_3$ thin films. Coherency of the twin boundaries were demonstrated with HRTEM. A misorientation between the matrix and the TTD is most likely responsible for the local amorphous regions along the (112) twin boundary. A very high density of order-disorder antiphase domains with structure steps of a/2<100> or a/2<100> plus a/2<110> across their boundaries were directly imaged with HRTEM. These structure steps are believed to be partially induced by the steps on the MgO substrate surfaces.

ACKNOWLEDGEMENT

This research is supported by the Office of Naval Research under contract N00014-88-K-0526. The authors would like to thank Dr. D. M. Maher and Dr. B. Yan for their useful discussions.

REFERENCES

1. Landolt-Bornstein, Group III, vol 16, p4R
2. A. I. Kingon, S. H. Rou, M. S. Ameen, T. M. Graettinger, K. D. Gifford, and O. H. Auciello, *Proceeding of American Ceramic Society*, 1989.
3. S. H. Rou, P. D. Hren, A. I. Kingon, "WORKSHOP ON SPECIMEN PREPARATION FOR TRANSMISSION ELECTRON MICROSCOPY OF MATERIAL II", (Mat. Res. Soc.), Spring 1990.
4. S. H. Rou, J. J. Hren, P. D. Hren, T. M. Graettinger, M. S. Ameen, O. Auciello, and A. I. Kingon, to be presented in XXII ICEM, Seattle, WA
5. S. Ogawa, D. Watanabe, H. Watanabe, and T. Komoda, Acta cryst., 11, 1958.

Chapter 4

Exerpted from

"Characterization of Perovskite Thin Films," Shang H. Rou, Ph. D. Thesis, North Carolina State University, Raleigh, NC 27695, 1990.

CHAPTER 5
MICROSTRUCTURAL CHARACTERIZATION OF THE EPITAXIAL (111) $KNbO_3$ ON (0001) SAPPHIRE

5.1. INTRODUCTION:

Sapphire is a common substrate employed for deposition of thin films for optical application [5.1-5.4] because it is transparent and relatively inexpensive compared with most other optically transparent substrates. Polycrystalline epitaxial (111) $KNbO_3$ thin films were deposited onto c-cut (0001) sapphire substrates using the processing technique described in Chapter 2. Electrooptic measurements were performed using a geometry with the laser normal to the $KNbO_3$ thin film and with the aluminum electrodes parallel to the substrate surface. We observed that the electrooptic coefficient for (111) $KNbO_3$ thin films were superior to that of the (100) oriented $KNbO_3$ thin films [5.5]. Therefore, (0001) sapphire is an important substrate for the deposition of $KNbO_3$ thin films.

This chapter discusses the microstructural characterization of (111) $KNbO_3$ on (0001) sapphire. Special types of boundaries, which we call multiple positioning boundaries (MPB's), were observed within (111) $KNbO_3$ thin films. These boundaries are the result of coalescence of the grains nucleated on different but equivalent sites. The atomic model for these types of MPB's showed a local lattice distortion which resulted in a misfit dislocation at the corners of MPB. Low angle grain boundaries were also observed within this film. Local strain field and misfit dislocations were observed along these boundaries.

Plan-view and cross-section TEM samples were prepared using a conventional method described by Summerville et al. [5.6]. In addition, lacquer was applied onto the thin film side of the plan view sample to avoid the redeposition of

molybdenum during ion milling. Warm acetone was then employed to remove the lacquer after the TEM sample developed perforation.

5.2. RESULTS AND DISCUSSION:

A selected area diffraction (SAD) pattern (figure 5-1a) was taken with the electron beam parallel to the sapphire [0001] zone axis. The (0001) sapphire and the (111) $KNbO_3$ were indexed using this pattern as illustrated in figure 5-1b. This SAD pattern demonstrated that the $KNbO_3$ thin film was epitaxially grown onto the sapphire substrate with the following orientation relationship:

(111) $KNbO_3$ // (0001) sapphire and [110] $KNbO_3$ // [1100] sapphire

This epitaxial relationship results in a lattice matching based on the second nearest neighbor atom between the overlayer and the substrate. Although the second order epitaxy is not the most energetically favorable match, the resultant small lattice mismatch minimizes the total interfacial energy.

We noticed that the $KNbO_3$ thin film diffraction spots were circumferentially elongated suggesting polycrystalline nature of the film. However, we only observed the (111) $KNbO_3$ diffraction pattern indicating that each $KNbO_3$ grain is epitaxial with respect to the substrate, and these epitaxial grains have a small in-plane orientation deviation among themselves.

Figure 5-2 shows the HRTEM micrograph of (111) $KNbO_3$ on (0001) sapphire. Morie' fringes combined with lattice fringes were observed within the same micrograph. As we know, Moire' fringes reveal the periodicity of misfit between two overlaying crystals [5.7]. The spacing of the Moire' fringes is approximately equivalent to eleven lattice fringes and is close to the theoretically predicted. It was noted that the lattice fringes exhibited a wavy characteristic. This could be attributed to a slight rotation between the $KNbO_3$ thin film and the sapphire

substrate. Defects on the substrate surface, which generate strain field and subsequentially distort the structure of substrate surface, are suspected to be the cause for this lattice rotation. This rotation of the epitaxial grains is consistent with the circumferentially elongated diffraction spots shown previously.

A cross sectional TEM micrograph is shown in figure 5-3. A sharp interface was observed between the $KNbO_3$ thin film and the sapphire substrate. This electron micrograph of the $KNbO_3$ thin film exhibited a polycrystalline type of contrast. The contrast could again be explained by a small orientation deviation among those epitaxy $KNbO_3$ grains. Because of the small orientation deviation among these $KNbO_3$ grains where the exact Bragg's condition could not be satisfied for some of the grains. This observation is consistent with the SAD pattern from a plan view TEM sample which shows circumferentially elongated $KNbO_3$ diffraction spots.

Top surfaces of (111) $KNbO_3$ thin films were observed to be rough as shown in figure 5-3. This can be an indication that the (111) $KNbO_3$ is not the most thermodynamically stable plane. One possible mechanism for forming this rough surface during growth is that once planes with other orientations, which are more thermodynamically stable than (111), appear, growth from these planes dominates. Therefore, the (111) $KNbO_3$ thin film exhibits rough surface with faceting. Orientation of these facets on the surface of the (111) $KNbO_3$ thin film is close to <100> zone axes of $KNbO_3$. The faceting of surface has been reported for the deposition of diamond thin films [5.8].

In general, the most close-packed plane is the most thermodynamically stable plane [5.9]. In perovskite structures, {100} planes have an interplanar spacing between the two nearest identical cation planes equivalent to the lattice constant of the pseudo-cubic unit cell. Similarly, the interplanar spacing for two

{111} planes having identical cation ion is equal to $\sqrt{3}/3*a$. The schematic comparison is shown in figure 5-4. Since the interplanar spacing is proportional to the atomic density of the particular plane, the (100) plane is more close-packed than the (111) plane and thermodynamically more stable. This can explain the observation of the (100) facets on the epitaxial (111) $KNbO_3$ thin film. Thin films of (100) $KNbO_3$ on (100) MgO [5.10] had a much smoother surface and a better uniformity than (111) $KNbO_3$ on (0001) sapphire. This rough surface with faceting of the (111) $KNbO_3$ thin film can be a serious drawback for channel waveguide applications.

Special types of boundaries were observed within the (111) $KNbO_3$ thin films. They are called multiple positioning boundaries (MPB's). These boundaries are formed as a result of coalescence of two adjacent grains which are initiated at equivalent but different positions on the substrate surface. MPB's are unique to epitaxial thin films [5.11]. The most common type of MPB is the double positioning boundary (DPB). This boundary is generated when (111) deposits are epitaxially grown onto a (111) or (0001) substrate. It is named "double positioning" because two equivalent but different nucleation positions are present on the substrate surface.

Epitaxial thin films of (111) $KNbO_3$ were deposited onto (0001) sapphire substrate. MPB's were observed within the epitaxial (111) $KNbO_3$ thin film. However, because of the special epitaxial relationship, a much more complex system of MPB's was observed.

In order to understand the MPB system within (111) $KNbO_3$ thin films, its layer structure and stacking sequence are described first (figure 5.5). Each individual layer contains only one cation element, K or Nb. Each Nb atom resides within a tetrahedral site of K sublattice and vice versa. These layers are arranged

with an alternate KNbKNb sequence. Because $KNbO_3$ is cubic, the site sequence of the (111) $KNbO_3$ layer structure is arranged with an abcabc fashion. A typical stacking sequence for (111) $KNbO_3$, which combines atomic and site sequences, is shown as follows:

a b c a b c a b c a b c a b c a b c a b c
K Nb K Nb K Nb K Nb K Nb K Nb K Nb K Nb K.

The layer structure of (0001) sapphire substrate shows that each layer contains only cations (Al) or anion (O). Because of the relative stability of the O layer over the Al layer, we surmise that it is oxygen, not aluminum, planes present on the sapphire substrate surface.

In order to simplify our analysis, we assume that the substrate surface was perfectly flat without a step. Furthermore, we ignored the energy differences by first overlaying either a K-O or a Nb plane on the sapphire substrate surface. Because Nb was the first component that was deposited onto the substrate surface, therefore the Nb plane was chosen as the first overlayer. This assumption may not be a valid one because there are potassium aluminate compounds [5.12-14] with small lattice mismatches (< 7%) with respect to the sapphire. Further experimental efforts are required to determine the role of interfacial chemistry in deposition of $KNbO_3$ on sapphire. In addition, the (0001) sapphire substrate is hexagonal; thus the cations Nb are energetically most stable sitting in the tetrahedral sites on the substrate surface.

As we mentioned previously, the overlayer (111) $KNbO_3$ exhibits a second order epitaxy with respect to the substrate. This epitaxial relationship leads to eight equivalent, but different nucleation positions on the substrate surface, as illustrated in figure 5-6. These eight nucleation positions can be divided into two groups. Each group contains four positions which show a <110> translation within

the 111 plane relative to each other on the substrate surface. And, the difference between the two groups is that there are two equivalent tetrahedral sites on the substrate surface. The stacking sequences for the nuclei, which initiated at eight equivalent but different positions on the substrate surface, are shown in figure 5-7.

Islands of (111) $KNbO_3$ randomly nucleated at eight equivalent but different positions on the (0001) sapphire substrate. As the islands grew larger, they eventually coalesced. A total of twenty eight different types of boundaries was generated. Because these boundaries were formed due to the eight different but equivalent positions available on the substrate surface, the proper name for them is "octuple positioning boundaries". Depending on the origination of nucleation positions for each two adjacent grains, these MPB's can be divided into three types, translational, double positioning, and translational double positioning boundaries, as depicted in table 6-1.

The first type of boundary, translational, results from two adjacent grains nucleated at same sites but with a <110> translational relationship with respect to another. Because stacking sequences for these two adjacent grains are identical, no difference could be observed within the reciprocal space. However, with the translational relationship between two adjacent grains and the discontinuity of the lattice periodicity near the boundary, we expect to observe the contrast and an atomic step at the translational boundary.

The second type of boundary, double positioning, results from two adjacent grains which nucleate from different sites and exhibit no translational relationship. Figure 5-8 illustrates the layer structure of DPB. Stacking sequences of these two adjacent grains across this DPB are different, so it can be distinguished in the reciprocal space along certain orientations. In fact, these two adjacent grains exhibit a twinning relationship with respect to each other.

The third type of boundary, translational double positioning, results from two adjacent grains which nucleate from different sites and also exhibit a <110> translation relationship relative to each other. Because these two adjacent grains have different stacking sequences and a discontinuous lattice periodicity across the boundary, these translational double positioning boundaries could be revealed in the reciprocal space and exhibit an atomic step when crossing the boundaries.

A SAD pattern (figure 5-9a) was taken along the [1010] sapphire zone axis. The illustration is shown in figure 5-9b. Indices were assigned to two sets of {110} $KNbO_3$ and the (1010) sapphire substrate. These two sets of {110} $KNbO_3$ electron diffraction patterns had a twinning relationship because a mirror reflection was exhibited across the {111} Bragg's reflection. We, therefore, know from figure 5-9a that either the DPB's, translational DPB's, or/and the {111} twin boundaries are present within this $KNbO_3$ thin film. A dark field image (figure 5-10), which was taken using a 110 Bragg reflection, revealed the contrast variation across the DPB or the translational DPB within the $KNbO_3$ thin film.

The atomic configuration of a DPB viewed along the sapphire [1010] zone axis is shown in figure 5-11. It is clearly shown in this schematic drawing that the DPB was formed by the coalescence of two regions with different stacking sequences. The mirror reflection was observed across this DPB. We know that this mirror reflection was the result of two different stacking sequences on the substrate surface. Double diffraction spots were observed in figure 5-8a. This suggests that the DPB's are not edge-on along this viewing orientation.

A possible translational boundary is shown in the dark field micrograph (figure 5-12). This micrograph suggests that two regions on both sides of the boundary had an identical orientation (stacking sequence) because no contrast was observed on both sides of the boundary. In addition, the contrast was enhanced

along the boundary. Based on our previous analysis, the contrast that we observed along the boundary could indicate that it is a translational boundary.

A high resolution electron micrograph (figure 5-13), which revealed two boundaries, X and Y, was taken with an electron beam parallel to the $KNbO_3$ [111] zone axis. The lattice exhibited a perfect periodicity across the boundary X. This perfect periodicity indicated that the boundary X is a DPB. Furthermore, this boundary exhibits a preferred direction along [211] which is a characteristic feature for DPBs [5.11]. The lattice showed an atomic step across the boundary Y. These atomic steps along this boundary strongly suggest that it is either a translational boundary or a translational DPB. We also observed from figure 5 13 that MPB's are not straight.

Figure 5-14 shows the proposed layer structure for DPB along <211>. With the proposed boundary structure, we found that the cations were unevenly distributed along this boundary. It is rather surprising that the HRTEM image of the DPB shows no lattice distortion with a minimum contrast. However, figure 5-13 shows that a slightly larger disorder region is exhibited near the translational boundary or the translational DPB compared with the region near the DPB. This observation suggests that the translational boundary or translational DPB is more energetic than the DPB.

Figures 5-10 and 5-12 revealed that the MPB's were wavy. In addition, the facets along these boundaries were (110) and (100) oriented. The reason for this wavy feature is not yet clear. Further detailed analysis is underway to understand these types of boundaries.

Multiple positioning boundaries are usually very energetic because of their incoherence [5.11]. Fullman [5.15] has performed a theoretical calculation to determine that the DPB has about 2/3 of energy of a high angle grain boundary.

Furthermore, Kong et al. [5.16] have reported that a high density of stacking faults was associated with the DPB. However, the high resolution micrograph (figure 5-13) shows a minimum contrast along this boundary. This result suggests that the DPB's within this material are not as energetic as we expected. The relatively low energy state could be because stability of $KNbO_3$ lattice is determined by locations of Nb ions. As we can see from the atomic configuration (figure 5-14), all the Nb ions remain within octahedral sites of oxygen sublattice, which is the most critical requirement for a stable $KNbO_3$. Therefore, these boundaries are relatively stable.

To our knowledge, no one has explained why multiple positioning boundaries prefer the <211> orientation. Researchers [5.17] have reported that because of the incoherence of these types of boundaries, they are highly mobile in some of the material systems. We believe that the motion of the DPB's took place via a diffusion process. As we can see from figure 5-14, with a <211> preferred orientation, the cations along these boundaries were arranged in a fashion which favored the movement of the boundary. The cations only need to hop a/6 <211> in order the DPB's to move. Minimum contrast and less distortion were observed along the <211> boundary.

A misfit dislocation, as indicated by the arrow in figure 5-13, was observed at the corner of the DPB. The atomic arrangement near the corner of the DPB is shown in figure 5-15. As we can see from this atomic arrangement, a lattice mismatch occurs when the DPB's turn from one [211] to another. This misfit dislocation was generated to release lattice mismatch at the corner of the DPB. This misfit dislocation may play a very important role in controlling the movement of the DPB's.

Effects of these types of boundaries on the ferroelectric and electrooptic properties is not known yet. However, the uneven distribution of the atomic density at the MPB's may shift cation atoms and generate a permanent dipole moment.

This residual dipole moment may act as either a ferroelectric domain nucleation site or a pinning site for the ferroelectric domain wall. We anticipate that the birefrigent shift will be affected.

Because of the small orientation deviation among those epitaxial grains, low angle tilt boundaries were observed within this thin film. Figure 5-16 shows the HRTEM micrograph of a low angle grain boundary. The two adjacent grains on both sides of this low angle grain boundary can, but do not necessarily, exhibit different stacking sequences. The tilt angle between these two grains is approximately 3°. The orientation of this low angle tilt boundary is also close to [211] $KNbO_3$. This could be an indication that the adjacent grains exhibit different stacking sequences on both sides of the low angle tilt boundary. A strain field was observed along the turning corner of this low angle tilt boundary. This strain contrast could be the result of a combination of the misfit induced by the two adjacent grains with different stacking sequences near the corner of the turning point and the angle misfit between two grains.

The dislocation array was arranged in a linear fashion. The core structure of the dislocation can clearly be seen in figure 5-16. It is worth noting that no amorphous phase was observed within this [211] low angle tilt boundary.

5.1. CONCLUSIONS:

The following conclusions can be drawn.

1. Epitaxial (111) $KNbO_3$ thin films were deposited onto (0001) sapphire substrates.
2. The (111) $KNbO_3$ thin films were polycrystalline with individual grains maintaining an epitaxial relationship with respect to the substrate.

3. The surface facets of (100) appeared on the top surface of the thin film because the (100)$KNbO_3$ is the most close-packed plane for $KNbO_3$.
4. Multiple positioning boundaries were observed within (111) $KNbO_3$ thin films. The MPB can be categorized into three types, translational, double positioning, and translational double positioning boundaries.
5. High resolution TEM revealed the contrast along the DPB's and that the misfit occurs at the turning corner along the DPB.
6. Low angle tilt grain boundaries were formed within the (111) $KNbO_3$ thin film, and the core structure of the misfit dislocation was observed.

5.4. REFERENCES:

[5.1] H. Adachi, T. Mitsuyu, O. Yamazaki, and K. Wasa, J. Appl. Phys , 60(2), 736(1986).

[5.2] H. Gotoh, T. Suga, H. Suzuki, and MN. Kimata, Jap. J. Appl. Phys. 20, L545 (1981).

[5.3] H. M. Manasevit and W. I. Simpson, J. Electrochem. Soc.: Solid State Science, Vol 116 No12, 1725 (1969).

[5.4] H. M. Manasevit, Journal of crystal growth, 55 , 1 (1981).

[5.5] T. M. Graettinger, S. H. Rou, M. S. Ameen, O. Auciello, and A. I. Kingon, submitted to Appl. Phys. Lett.

[5.6] M. K. Summerville and J. B. Posthill, Journal of Electron Microscopy Technique, vol 12, 56(1989).

[5.7] D. W. Pashley, In "Thin films," ASM, 59 (1964)

[5.8] K. Kobashi, K. Nishimura, Y. Kawate, and T. Horiuchi, Physical Review B, vol38 no6, 4067

[5.9] C. R. Barrett, W. D. Nix, and A. S. TEtelman, The Principle of Engineering Materials.

[5.10] Unpublished data.

[5.11] J. W. Matthews, Epitaxial Growth, 465.

[5.12] Brownmiller, Am. J. Sci., 29, 266 (1935).

[5.13] Yamaguchi, Suzuki, Bull. Chem. Soc. Jpn, 41, 93 (1973)

[5.14] D. Dyson, Johnson, Trans. J. Br. Ceram. Soc., 72, 49 (1973)

[5.15] R. L. Fullman, J. Appl. Phys., 22, 448 (1951).

[5.16] H. S. Kong, J. T. Glass, and R. F. Davis, J. Mater. Res., vol. 4, No 1, 204 (1989).

[5.17] M. J. Stowell and T. J. Law, Phys. Status Solidi, 16, 117 (1966).

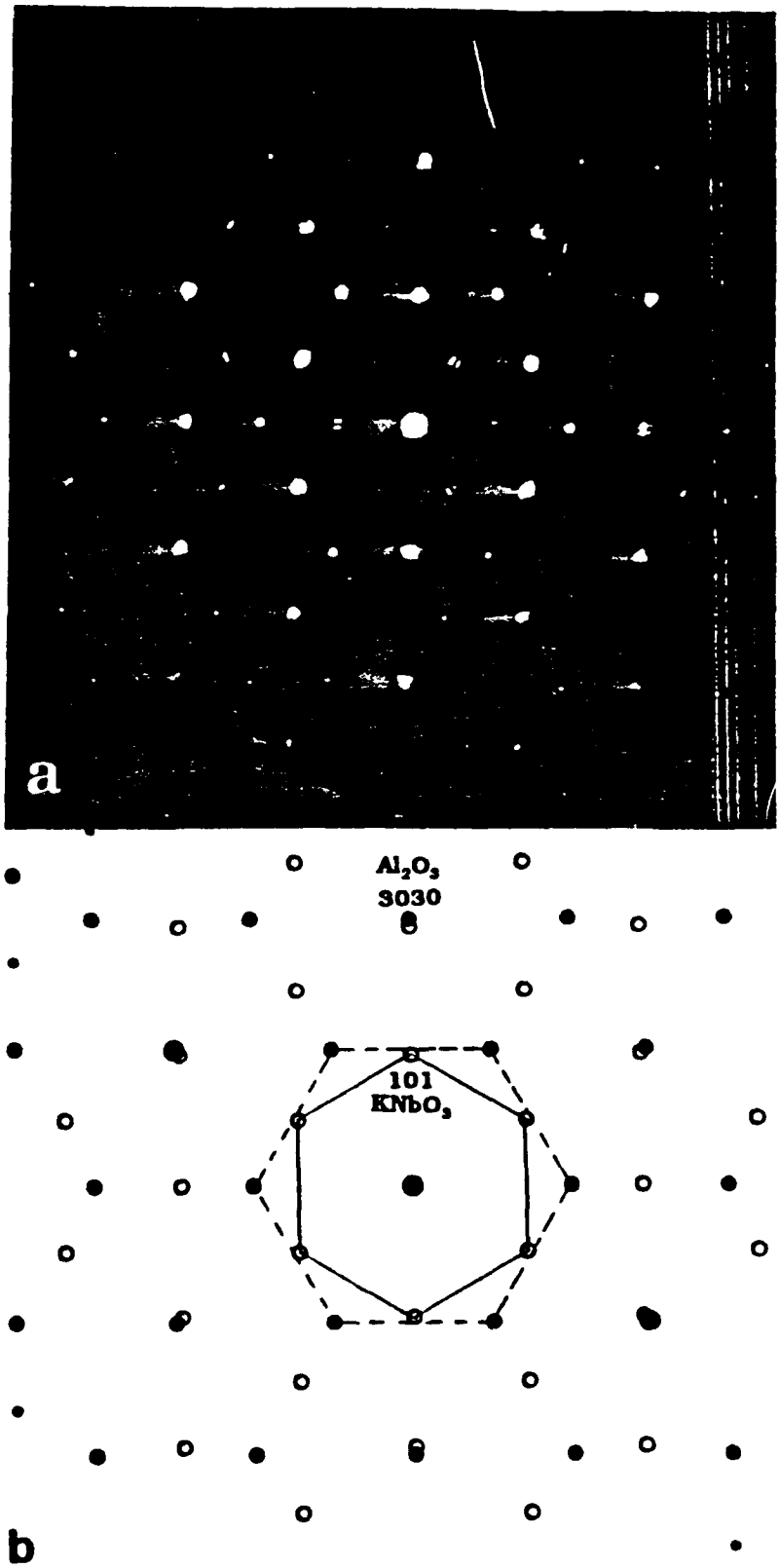

Figure 5-1 a) A SAD pattern with the electron beam along sapphire [0001] zone axis.

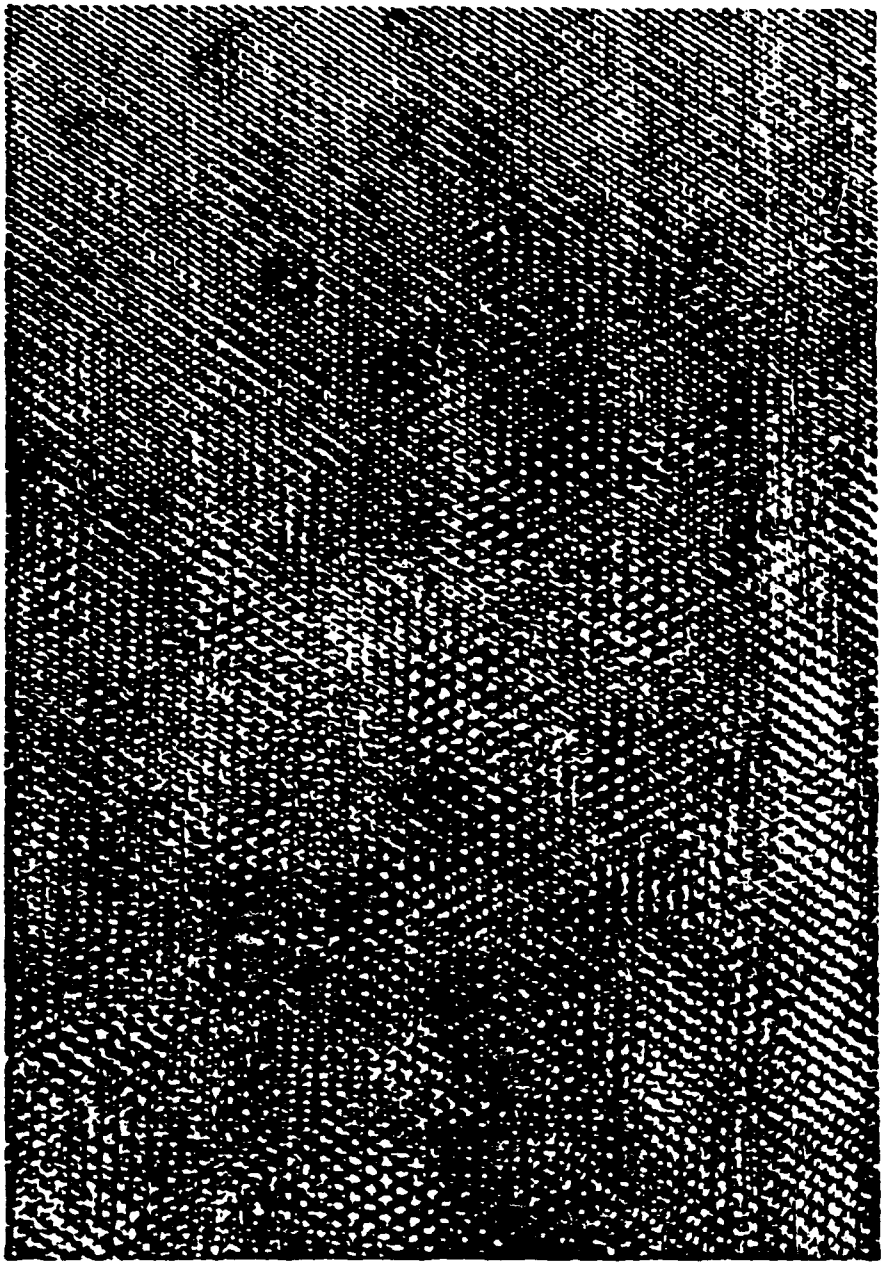

Figure 5-2 A high resolution micrograph exhibiting Moire fringes and lattice fringes.

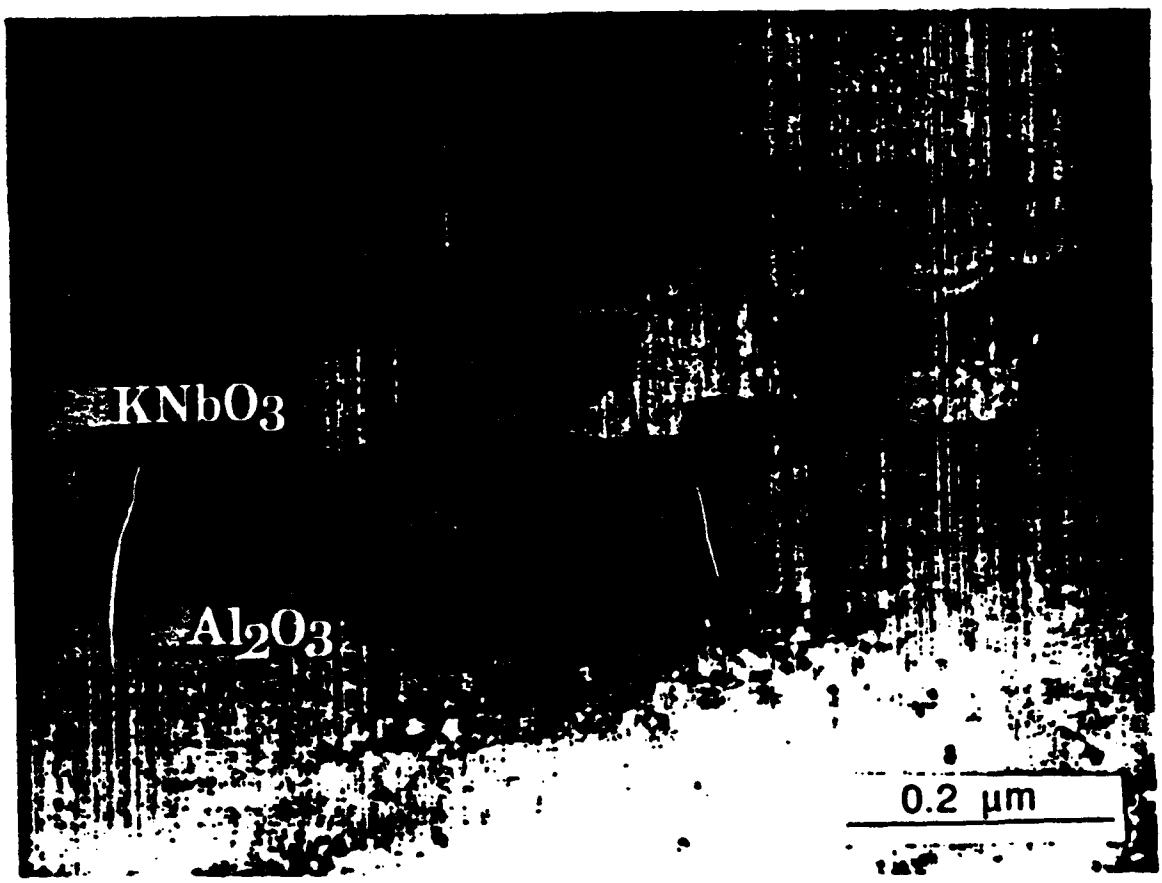

Figure 5-3 A cross section TEM micrograph of (111) $KNbO_3$ on ((0001) sapphire.

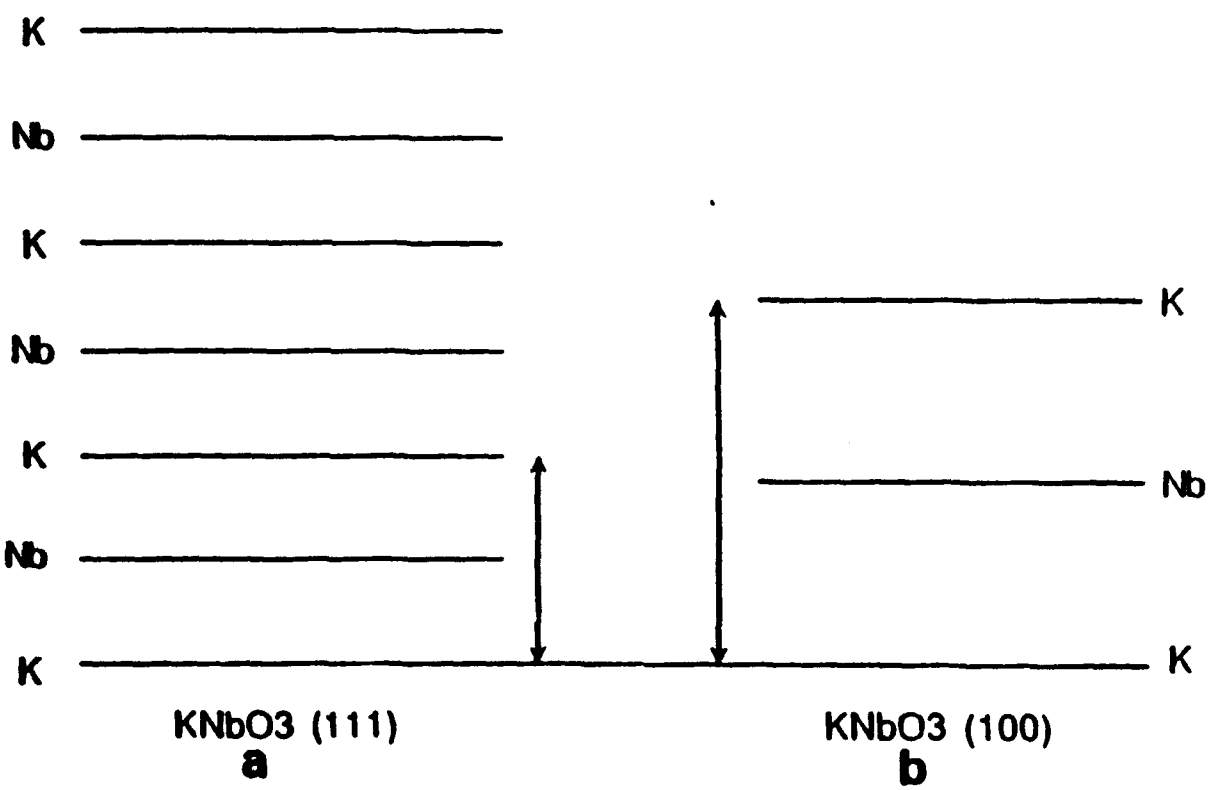

Figure 5-4 Illustration of the interplanar spacings for a) (111) $KNbO_3$ and b) (100) $KNbO_3$.

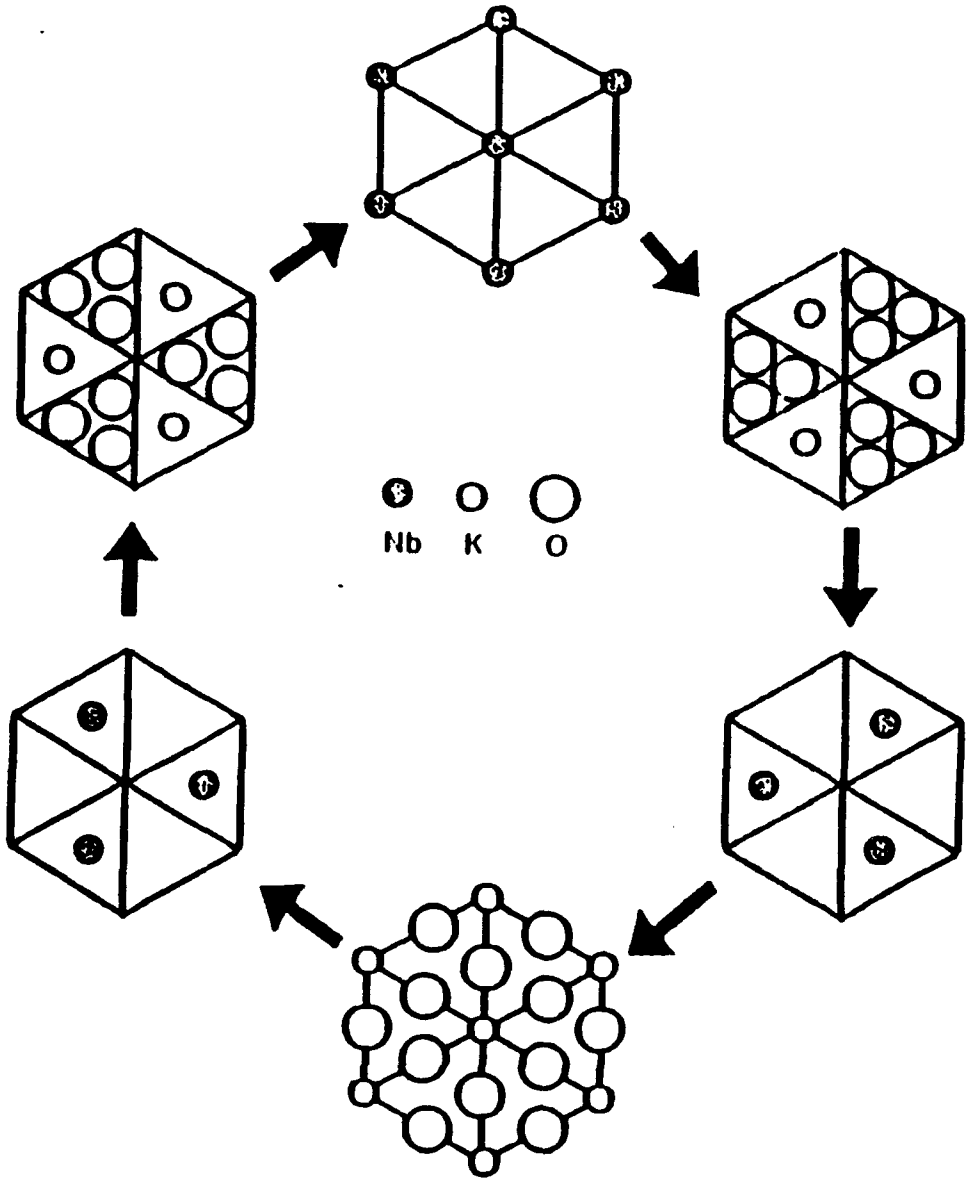

Figure 5-5 Layer structure of KNbO3 viewed along [111] zone axis

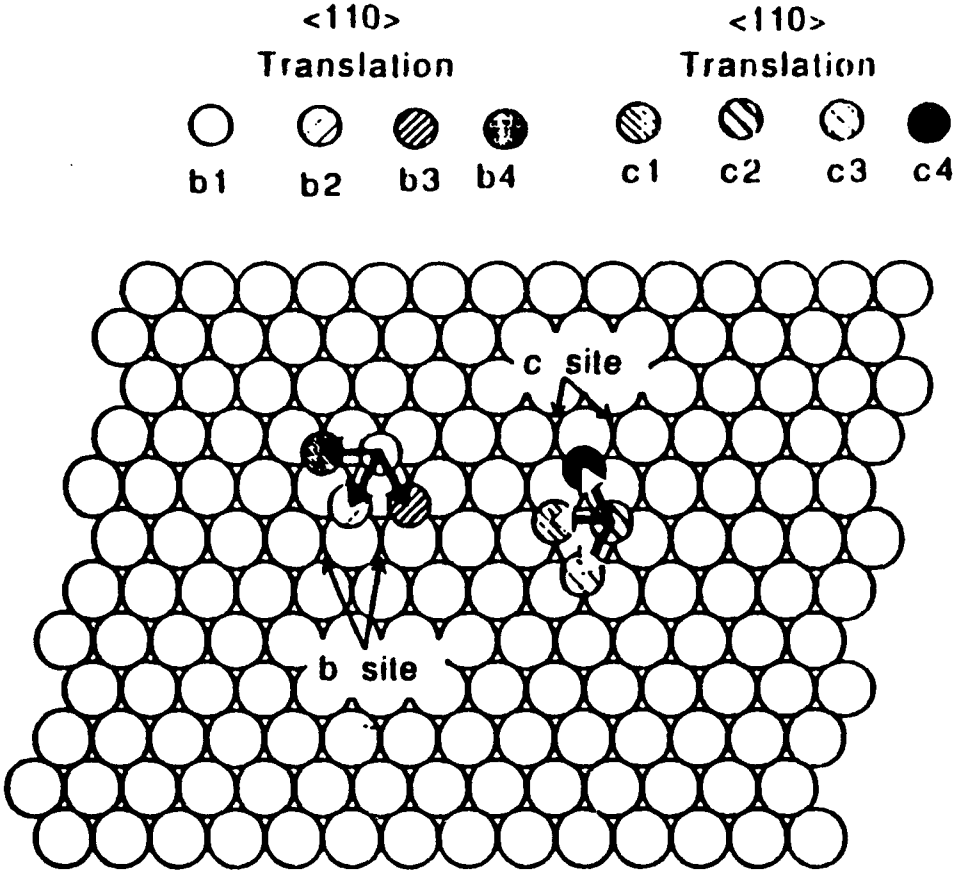

Figure 5-6 Illustration of two groups of equivalent but different nucleation sites on the substrate surface.

a1	a2	a3	a4		b1	b2	b3	b4
c1	c2	c3	c4		a1	a2	a3	a4
b1	b2	b3	b4		c1	c2	c3	c4
a1	a2	a3	a4		b1	b2	b3	b4
c1	c2	c3	c4		a1	a2	a3	a4
b1	b2	b3	b4		c1	c2	c3	c4

Figure 5-7 The stacking sequences of eight nuclei from eight equivalent but different sites.

Type of Boundary	Translational Boundary	DPB	Translational DPB
Site	Same	Different	Different
Translation	<110>	No	<110>
Number of Possibility	12	4	12
Typical Example	c_1 c_2 b_1 b_2 a_1 a_2 Substrate	c_1 c_1 b_1 a_1 a_1 b_1 Substrate	c_1 c_2 b_1 a_2 a_1 b_2 Substrate

Table 6-1 Different types of multiple positioning boundaries.

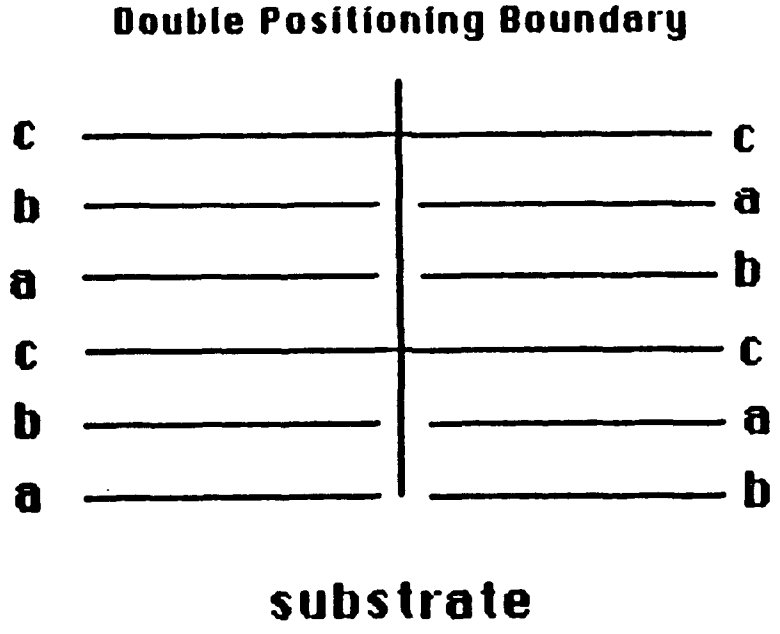

Figure 5-8 The stacking sequence for a DPB.

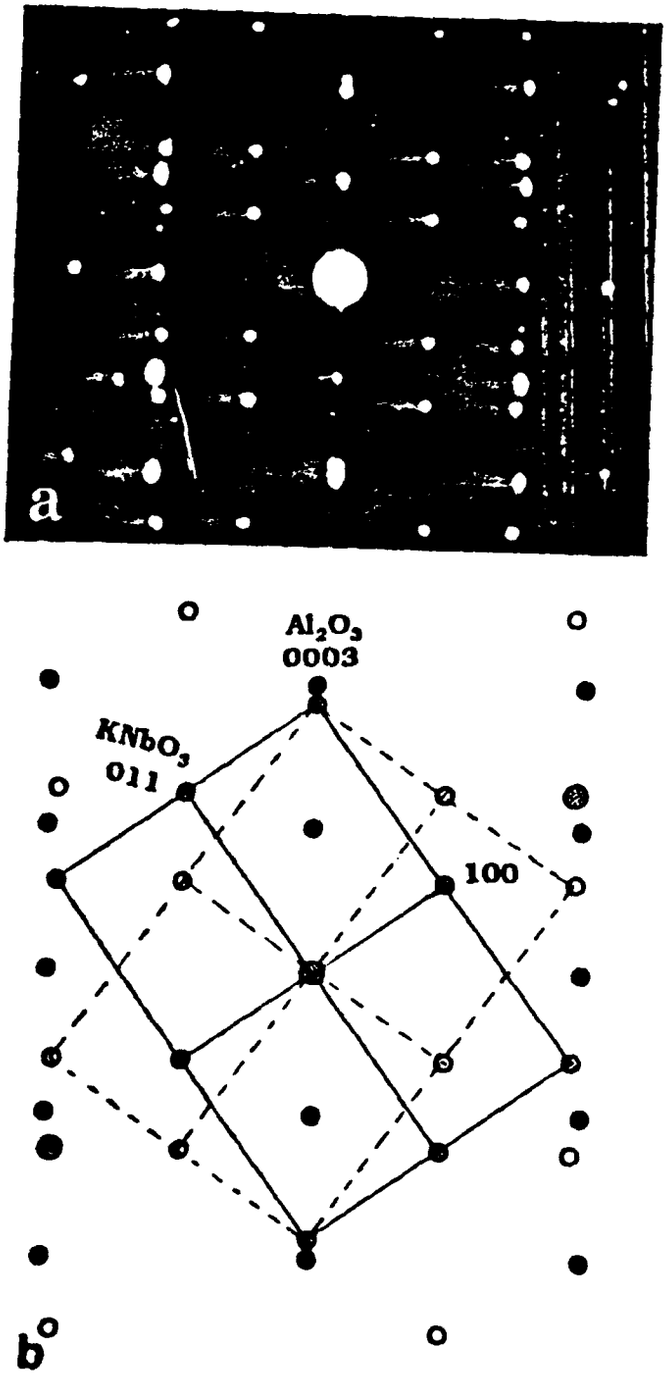

Figure 5-9 A SAD pattern along the sapphire [1010] zone axis.

Figure 5-10 A dark field micrograph of $KNbO_3$ using a 110 reflection, showing the DPB's.

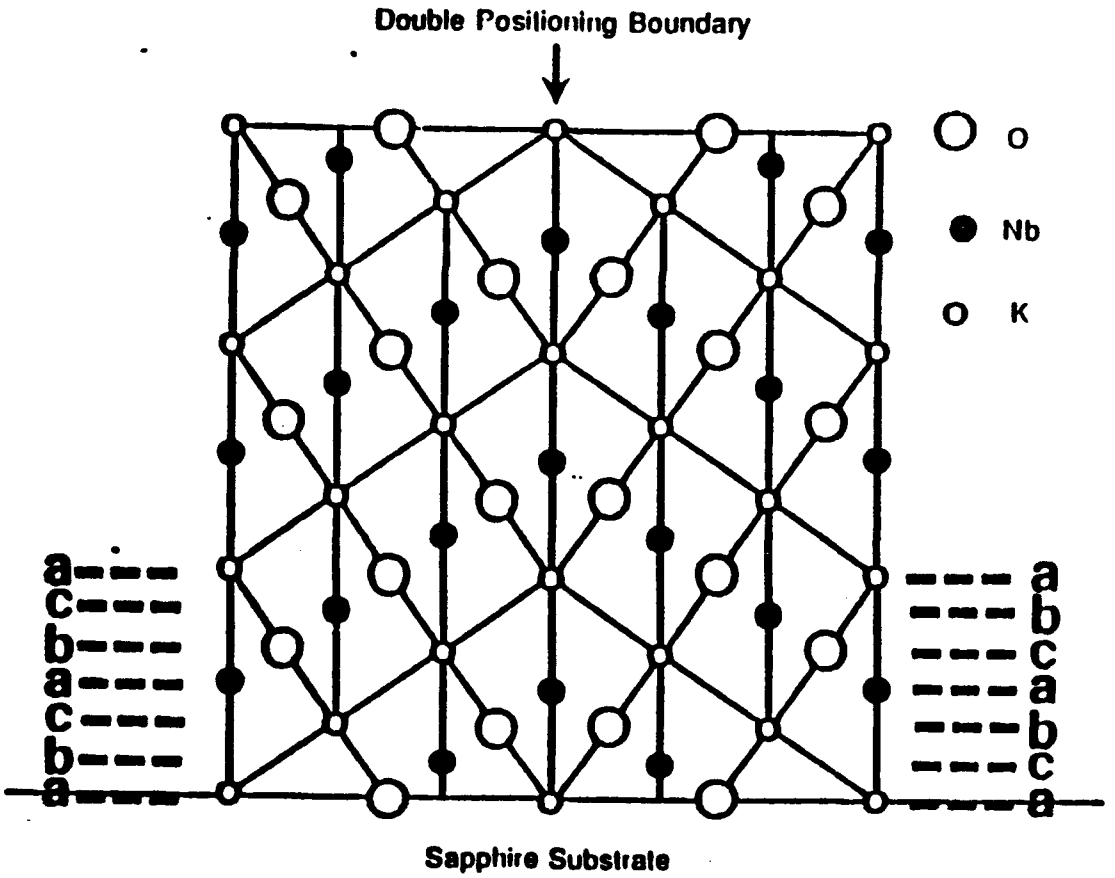

Figure 5-11 The atomic configuration of a DPB viewed along (1010) substrate.

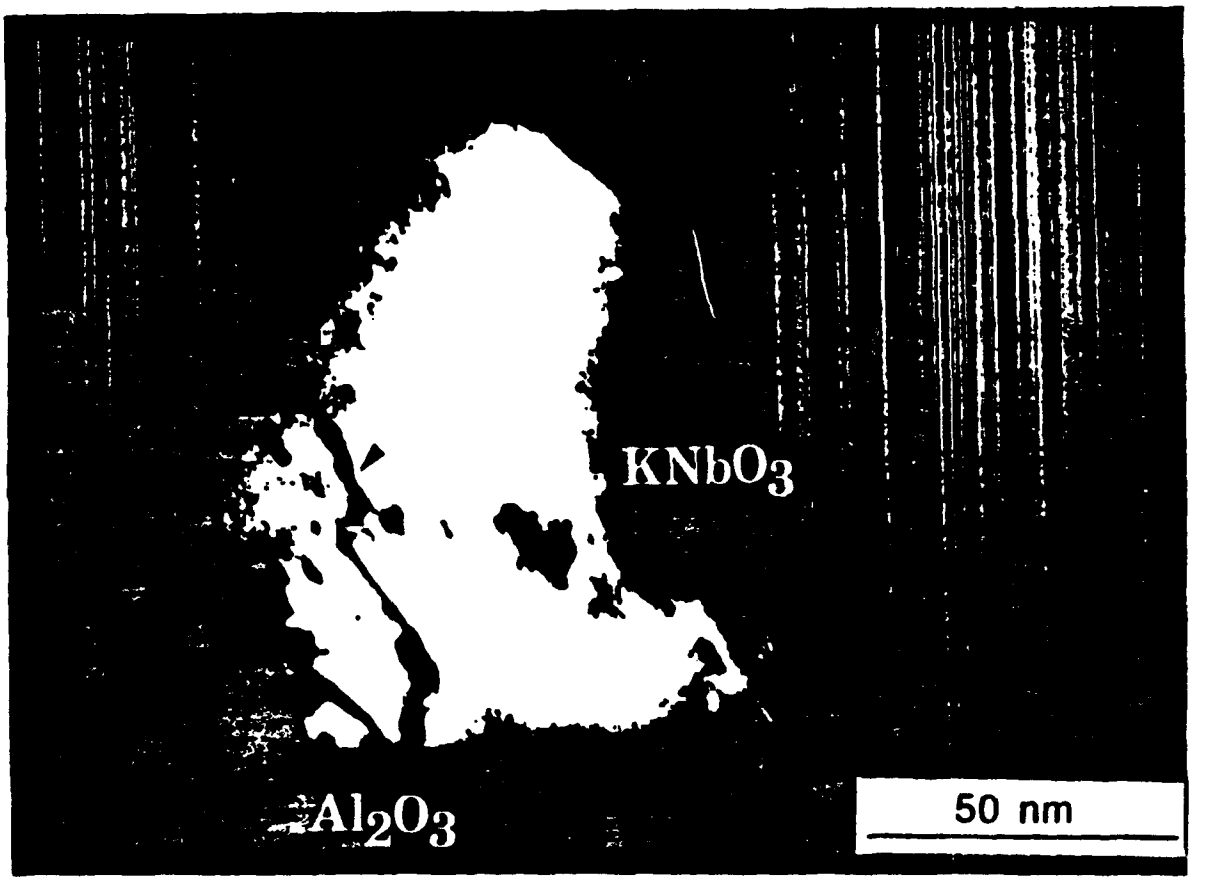

Figure 5-12 A dark field micrograph, showing an translational boundary

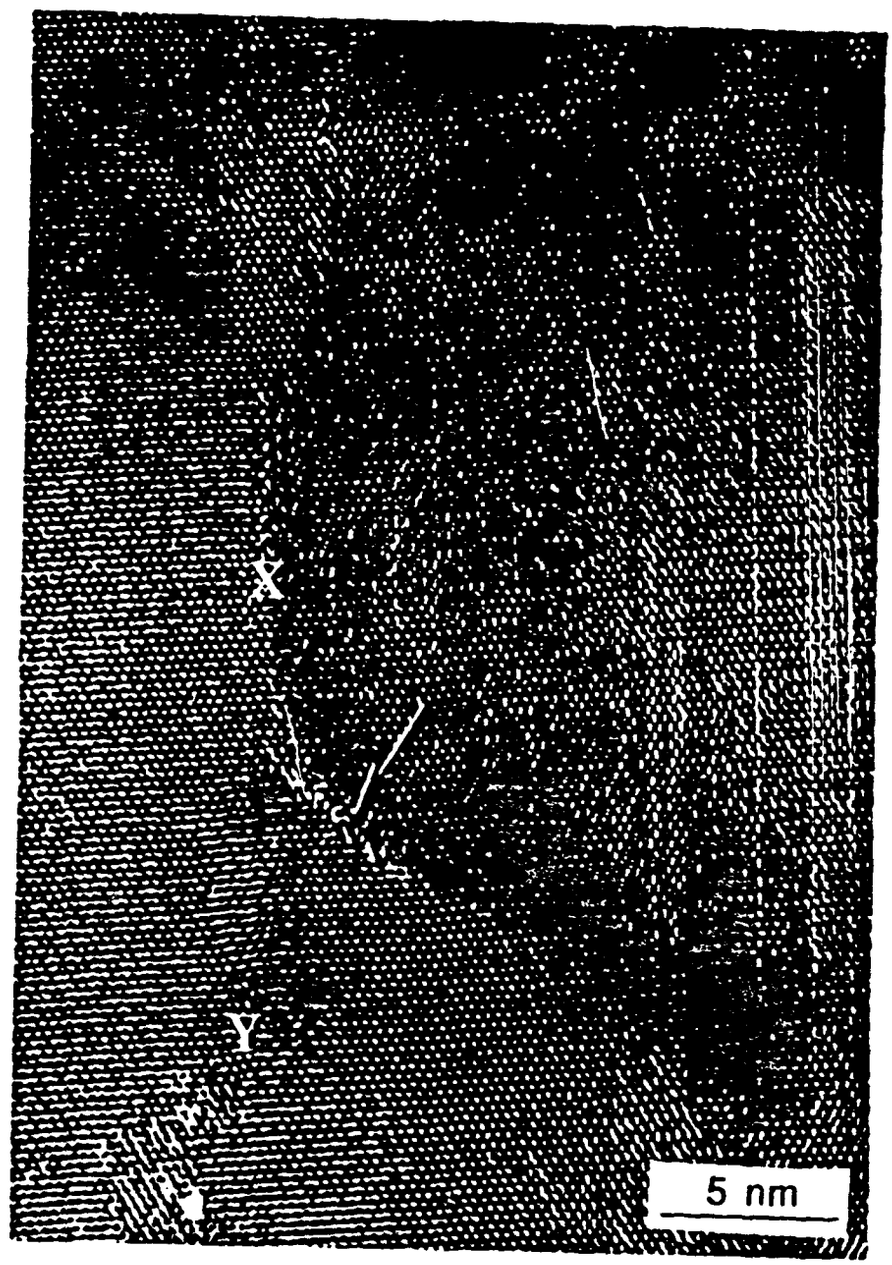

Figure 5-13 A HRTEM image of MPB's viewing along $KNbO_3$ [111] zone axis.

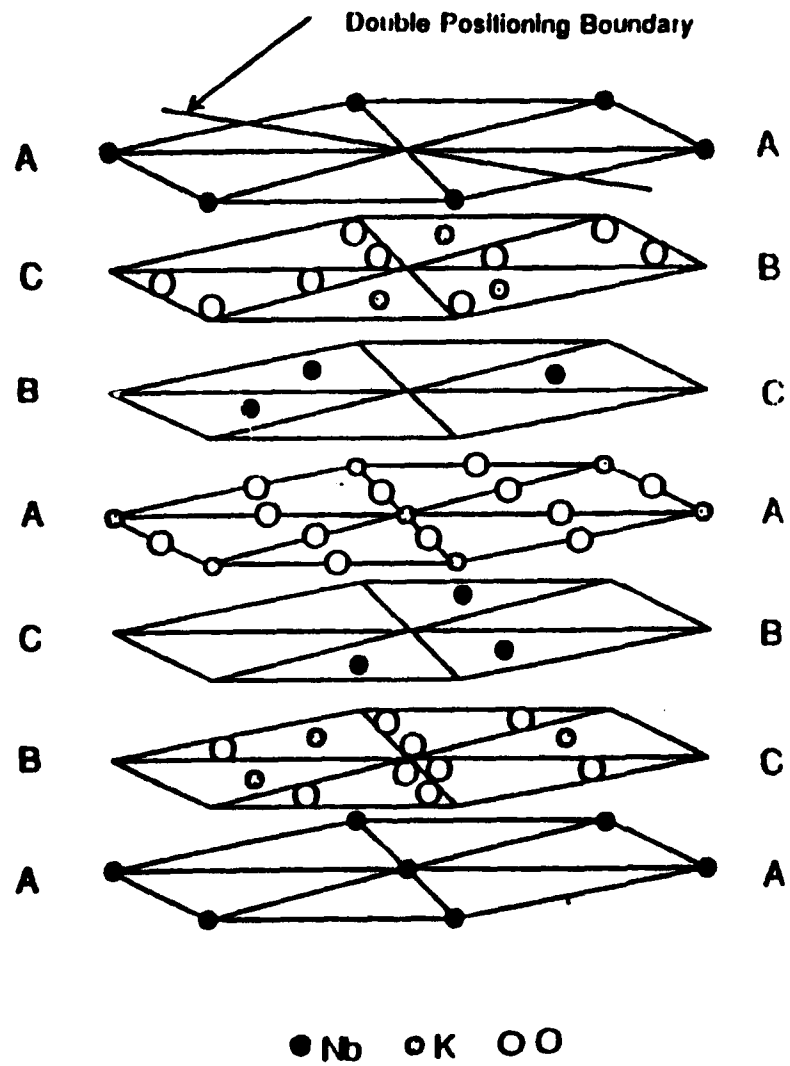

Figure 5-14 The layer structure of a DPB along the [211] orientation.

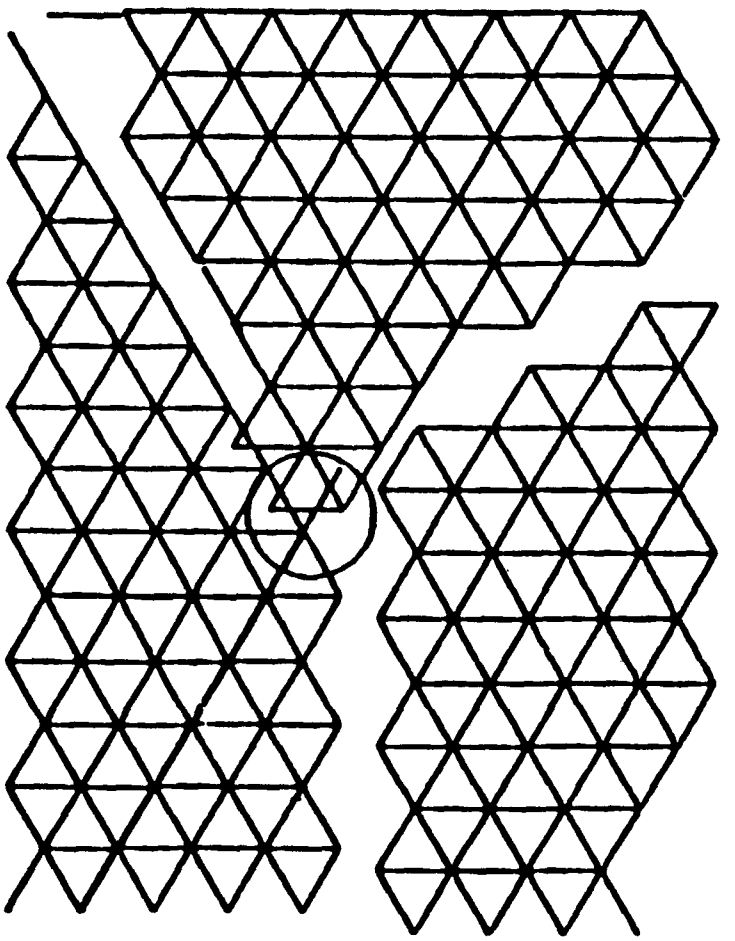

Figure 5-15 The atomic arrangement close to the turning corner of the DPB.

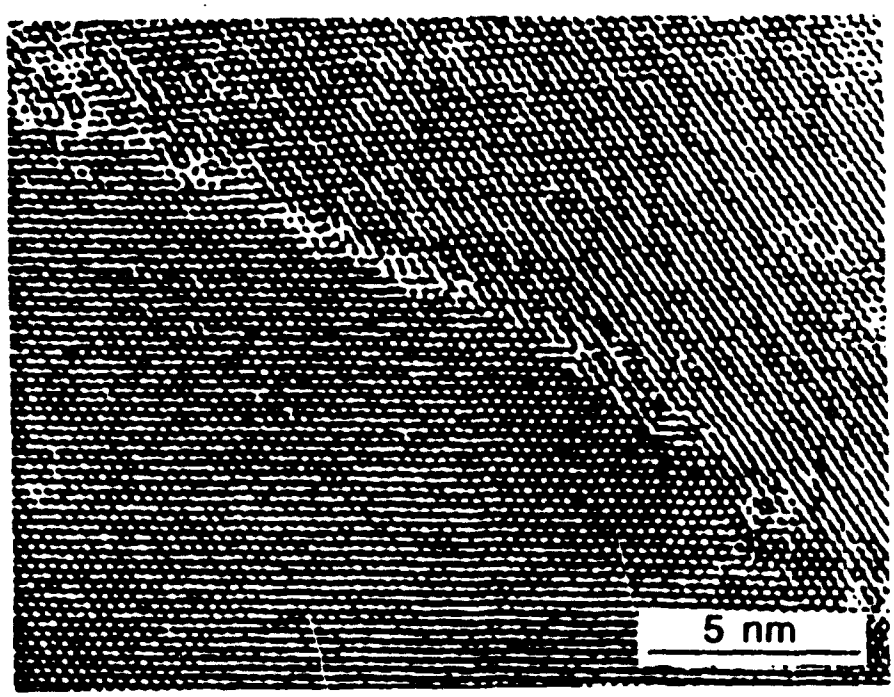

Figure 5-16 The HRTEM micrograph showing a low angle grain boundary.

Chapter 5

Reprinted from

"Electro-optic characterization of ion beam sputter-deposited $KNbO_3$ thin films," T. M. Graettinger, S. H. Rou, M. S. Ameen, O. Auciello, and A. I. Kingon, Appl. Phys. Lett., **58**(18), 1991, pp. 1964-1966.

Electro-optic characterization of ion beam sputter-deposited $KNbO_3$ thin films

T. M. Graettinger, S. H. Rou, M. S. Ameen,[a] O. Auciello,[b] and A. I. Kingon
Department of Materials Science and Engineering, North Carolina State University, Raleigh, North Carolina 27695-7919

(Received 31 October 1990; accepted for publication 5 February 1991)

The electro-optic properties of potassium niobate thin films deposited using a computer-controlled ion beam sputtering technique have been studied for the first time. Epitaxial and polycrystalline films were deposited on single crystal magnesium oxide and highly (111) oriented films were deposited on sapphire for the study. All films exhibited a quadratic-like dependence of birefringence shift on the applied electric field. The microstructure of the films and its relation to the observed electro-optic properties is discussed.

Ferroelectric materials are currently receiving much attention in electronic materials research. One subset of particular interest is those materials suitable for integrated electro-optic applications. This class of ferroelectrics includes the well known materials barium titanate, lead lanthanum zirconate titanate (PLZT), and lithium niobate as well as potassium niobate which is reported in the present study.

Potassium niobate has been identified as a candidate for high-speed electro-optic applications. It possesses a high electro-optic coefficient ($r_{42} = 380 \times 10^{-12}$ m/V)[1] and a moderate dielectric constant ($\epsilon_{42} = 137$),[2] both desirable characteristics for high speed applications. These properties rank $KNbO_3$ at the top of Tuttle's figure of merit comparison[2] and Holman's device-level analysis[3] of materials in this class including barium titanate, PLZT, and lithium niobate. Large, high-quality crystals of $KNbO_3$ have been difficult to grow, with the greatest success coming from the top-seeded solution technique.[4]

Thin-film processing techniques offer several advantages over bulk crystal growth in the fabrication of optical quality $KNbO_3$. These include precise compositional control and the ability to utilize low growth rates. Thin-film vapor deposition will not limit compound formation to formation from K_2O-rich phases, as is the case for bulk crystal growth. The lower growth rates can lead to lower defect densities and improved compositional control.

A computer-controlled ion beam sputter deposition system has been developed for the fabrication of thin film oxide materials.[5] For the synthesis of $KNbO_3$ a sequential layer-by-layer deposition scheme is used. Very thin (5–20 Å) alternating layers are deposited by sputtering metallic Nb and pressed powder potassium superoxide (KO_2) targets held in Nb rings and mounted to the arms of a rotating target holder. At the deposition temperatures used, typically 450 to 650 °C, these layers interdiffuse and react to form $KNbO_3$ films.

A quartz crystal resonator (QCR) provides continuous deposition feedback to a system control computer. A deposition program has been written using the software package LabView[6] that converts the resonator feedback to the amount of material deposited from the target. When this amount reaches a predetermined setpoint, the ion beam pulses off, the high-vacuum stepper motor rotates the next target into position in front of the ion source, and the ion beam then pulses back on. Layers of Nb and K are deposited repeatedly with interdiffusion between the layers occurring until the desired film thickness (typically 2000–6000 Å) is reached. Adjustment of the computer parameters, and thus the thicknesses of the Nb and K layers, allows fine compositional changes to be made in deposited films.

Substrates are mounted on an inconel plate which is mounted on top of a furnace assembly. The heater element is a 500 W quartz lamp which is capable of heating the surface of the substrate to 800 °C. A type R thermocouple is secured to the surface of a dummy substrate which is also mounted to the surface of the inconel plate. Films have been grown on substrates of single-crystal MgO and sapphire as well as fused silica and SiO_2/Si at deposition temperatures between 450 and 650 °C.

Films are routinely analyzed using x-ray diffraction (XRD) following deposition to determine the crystalline nature of the films. Energy dispersive x-ray spectroscopy (EDS), scanning Auger electron microscopy (SAM), and Rutherford backscattering (RBS) techniques have been used for compositional analysis. Transmission electron microscopy (TEM) has been used for further microstructural characterization.

Electro-optic measurements have been made on films deposited on transparent substrates so the laser light can pass perpendicularly through the films. Two 1 mm × 5 mm aluminum electrodes 1 mm apart were sputter deposited on top of the films for these measurements. An electric field up to 3 kV/mm could be applied across the electrodes using a high-voltage power supply. The relative shift of the phase retardation is measured versus applied voltage using the system shown in Fig. 1 which was adapted from the work by Adachi *et al.*[7]

Single-crystal MgO(100) substrates have been used extensively for the deposition of $KNbO_3$ thin films. By adjusting deposition parameters a series of $KNbO_3$ microstructures have been produced. This series of films has been critically analyzed and the microstructural defects characterized.[8,9] Substrate temperature during deposition

[a]Currently Materials Research Corporation, Orangeburg, NY 10962.
[b]Also Microelectronics Center of North Carolina, Research Triangle Park, NC 27709-2889.

 0003-6951/91/181964-03$02.00

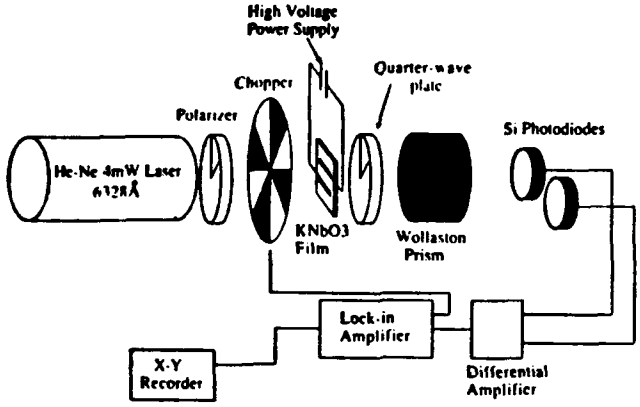

FIG. 1. Configuration of the optical system used to measure the birefringence shift of electro-optic thin films.

has been found to play the most important role in determining the microstructure of deposited films. $KNbO_3$ films deposited at 500 °C on MgO have been amorphous. By raising the substrate temperature to 550 °C polycrystalline films were produced. The grains were approximately 0.5 μm in size and some grains possessed an epitaxial relationship to the substrate. Fully epitaxial, mostly single-crystal films were produced at 600 °C. Tetrahedral twin domains have been found to be present in these films.[9,10] The number of twin domains present in the films has been directly correlated to ⟨110⟩ steps on the MgO surface. Therefore, a surface preparation technique has been developed consisting of a chemical etch followed by a high-temperature anneal that reduces the number of these steps and, hence, the twin density in the films.

High-quality films have also been deposited on Si/SiO_2 and sapphire (0001). Again, substrate temperature was found to be the most important parameter influencing the microstructure of $KNbO_3$ films. At 500 °C films deposited on Si were amorphous. Microcrystalline $KNbO_3$ in an amorphous matrix resulted from a Si substrate temperature of 550 °C, and polycrystalline films exhibiting little orientation were deposited at 600 °C.

$KNbO_3$ has been deposited on sapphire (0001) substrates at 600 °C. These films were highly (111) oriented. Growth-related stacking faults which lead to multiple positioning boundaries have been found in the microstructure of these films.[11] In addition, local strain fields and misfit dislocations were observed along low angle grain boundaries.

For measurement of the electro-optic properties, light was passed through the films perpendicular to the film plane. Measurements were thus limited to films on transparent substrates, i.e., films on MgO and sapphire. He-Ne laser light was polarized at 45° to the direction of the applied electric field and passed through the film. Two photodiodes were used to measure the rotation of the angle of polarization. $\Delta\theta$. The phase retardation, $\Delta\delta$ is found to be twice $\Delta\theta$. The birefringence shift $\Delta(\Delta n)$ can then be calculated as

$$\Delta(\Delta n)=\lambda\Delta\delta/2\pi d, \quad (1)$$

TABLE I. Comparison of $KNbO_3$ to other thin-film electro-optic materials.

Film, orientation	R (10^{-17} m^2/V^2)	Estimated dielectric constant
PLZT (28/0/100) (111)	0.5–6	2000
PLZT (28/0/100) (100)	4.43	2000
PLZT (9/65/35) (110)	0.55–10	1000
$KNbO_3$, (111)	5.5	< 100
$KNbO_3$, (100)	0.09–0.3	< 100

where λ is the wavelength of the laser (6328 Å) and d is the film thickness. Figures 2(a), 2(b), and 2(c) show the birefringence shift plotted versus the applied electric field for $KNbO_3$ films deposited on MgO substrates. Figure 2(a) shows the result for a polycrystalline $KNbO_3$ film. This film exhibited some hysteresis as the electric field was applied and removed. Hysteresis of this type is common in ferroelectric materials and arises due to ferroelectric domain wall motion. However, the magnitude of the observed birefringence shift is small for these polycrystalline films.

Epitaxial $KNbO_3$ films deposited on MgO were measured and the results are presented in Figs. 2(b) and 2(c). The magnitude of the birefringence shift is greater than the case of the polycrystalline films. A slight increase in the magnitude of the birefringence shift is observed for the films deposited on MgO substrates that have undergone the surface preparation procedure. These findings support preliminary conclusions that the observed inversion domain boundaries and/or tetrahedral twin domains inhibit domain wall movement in the films, thus decreasing the magnitude of the electro-optic effect.

Crystal orientation is primarily determined by the substrate. Films deposited on sapphire were highly oriented in the (111) direction allowing for the measurement of $KNbO_3$'s electro-optic properties in a different crystallographic direction than the (100) films on MgO. Figure 2(d) shows the electro-optic characteristics of the films deposited on sapphire. The (111) orientation of the films makes use of the shear modes of the electro-optic tensor for $KNbO_3$. In the case of the reported linear electro-optic coefficients, it is the shear modes which have the largest values. Figure 2(d) illustrates that the birefringence shift at 2 kV/mm is an order of magnitude greater for the films on sapphire than for films on MgO. This result compares very favorably with previous measurements by other investigators of PLZT films.[12,13] Like the polycrystalline film on MgO, the film on sapphire exhibited hysteretic behavior, though to a greater extent in the latter case. Table I compares the effective quadratic electro-optic coefficient R of PLZT thin films found in the recent literature with the $KNbO_3$ films studied here assuming a quadratic dependence on the applied field. No direct comparison is made to bulk $KNbO_3$ since only linear coefficients have been routinely reported for single domain material. As the films studied are multidomain material and domain reversal is expected, the quadratic-like dependence of birefringence shift on applied field is expected. In addition, Table I contains estimates of the dielectric constants for these films.

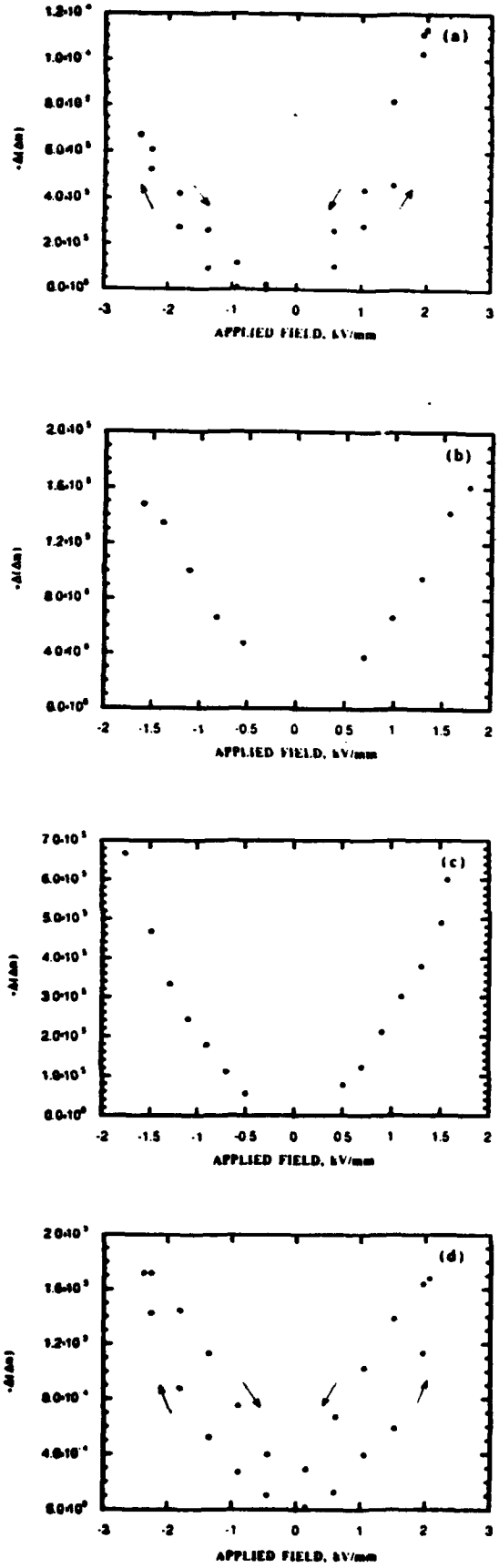

FIG. 2. The birefringence shift is plotted vs applied field for (a) polycrystalline $KNbO_3$ on MgO, (b) epitaxial $KNbO_3$ on unprepared (100) MgO, (c) epitaxial $KNbO_3$ on prepared (100) MgO, and (d) highly (111) oriented $KNbO_3$ on (0001) sapphire.

Combining the low dielectric constants of $KNbO_3$ with the electro-optic coefficients which are comparable to PLZT, makes $KNbO_3$ films better suited for high-speed switching applications.

In summary, high-quality $KNbO_3$ films were deposited on silicon, sapphire and single-crystal MgO substrates using a computer-controlled ion beam sputter-deposition system. Thin layers of niobium and potassium superoxide (KO_2) were sequentially deposited and continuously interdiffused at the chosen substrate temperatures to produce films of potassium niobate. The birefringence shift of all $KNbO_3$ films was measured and displayed a quadratic-like dependence on the applied electric field, as expected for multi-domain material. Crystal orientation, determined via the substrate type (MgO or sapphire), has a very large effect on the birefringence shift measured. The microstructural defects also influence the shift, but to a much smaller extent. $KNbO_3$ films on sapphire showed the largest electro-optic effects and compare well with PLZT films fabricated by other groups. This effect combined with the relatively low dielectric constant of $KNbO_3$ makes these films strong candidates for high-speed switching applications in the future.

The authors would like to acknowledge the Office of Naval Research for support of this work, the National Defense Science and Engineering Graduate Fellowship program for support of one of the authors (TMG), Leybold Inficon for use of a prototype quartz crystal resonator, Dr. Klaus J. Bachmann for helpful discussions concerning the optical measurements, Dr. C. E. Land for useful discussions about ferroelectric properties, and Dr. Alan R. Krauss for fundamental contributions to the development of the ion beam sputter-deposition technique.

[1] Landolt-Bornstein, *New Series, Group III* (Springer, New York, 1981), Vol. 16, pt. A.
[2] B. Tuttle, MRS Bulletin Oct./Nov., (1987), pp. 40–45.
[3] R. Holman, L. Althouse Johnson, and D. Skinner, in *Proceedings of the Sixth IEEE International Symposium on Applied of Ferroelectrics* (IEEE, New York, 1986) pp. 32–41.
[4] W. Xing, H. Looser, H. Wüest, and H. Arend, J. Cryst. Growth 78, 431 (1986).
[5] A. I. Kingon, S. H. Rou, M. S. Ameen, T. M. Graettinger, K. Gifford, O. Auciello, and A. R. Krauss, in *Ceramic Transactions*, Vol. 14: Electrooptics and Non-Linear Optic Materials, edited by A. S. Bhalla, E. M. Vogel, and K. M. Nair (American Ceramic Society, Westerville, Ohio, 1990), pp. 179–196.
[6] National Instruments Corporation, Austin, TX 78730-5039.
[7] H. Adachi, T. Kawaguchi, K. Setsune, K. Ohji, and K. Wasa, Appl. Phys. Lett. 42, 867 (1983).
[8] A. I. Kingon, M. S. Ameen, O. Auciello, K. Gifford, H. Al-Shareef, T. M. Graettinger, S. H. Rou, and P. Hren, Second Symposium on Integrated Ferroelectrics, Monterey, March 1990 (to be published in J. Ferroelectrics).
[9] S. H. Rou, J. J. Hren, P. D. Hren, T. M. Graettinger, M. S. Ameen, O. Auciello, and A. I. Kingon, Materials Research Society Symposium Proceedings, Vol. 183 (MRS, Pittsburgh, PA, 1990), pp. 285–290.
[10] S. H. Rou, J. J. Hren, P. D. Hren, T. M. Graettinger, M. S. Ameen, O. Auciello, and A. I. Kingon, *Electron Microscopy* 1990: *Proceedings of the XIIth International Congress for Electron Microscopy*, Vol. 4, Material Sciences (San Francisco, San Francisco, CA, 1990), pp. 466–467.
[11] S. H. Rou (unpublished).
[12] M. Ishida, S. Tsuji, K. Kimura, H. Matsunami, and T. Tanaka, J. Cryst. Growth 45, 393 (1978).
[13] H. Adachi, T. Mitsyu, O. Yamazaki, and K. Wasa, J. Appl. Phys. 60, 736 (1986).

Chapter 6

Reprinted from

"Optical characterization of potassium niobate thin film planar waveguides," T. M. Graettinger and A. I. Kingon, MRS Symposium Proceedings, Vol. 243, *Ferroelectric Thin Films II*,(MRS, Pittsburgh, PA), 1991 (in press).

OPTICAL CHARACTERIZATION OF POTASSIUM NIOBATE THIN FILM PLANAR WAVEGUIDES

THOMAS M. GRAETTINGER AND A. I. KINGON
North Carolina State University
Dept. of Materials Science and Engineering
Raleigh, NC 27695-7919

ABSTRACT

Initial results of the waveguiding properties of $KNbO_3$ thin films are presented. The refractive indices of epitaxial films deposited on single crystal magnesium oxide substrates have been measured. Additionally, these films have been used as the basis for modelling a potassium niobate thin film phase modulator. Results of the model are compared with existing technology.

INTRODUCTION

Ferroelectric materials possess great potential for use in integrated optics due to their strong electro-optic and non-linear optical effects. Thin film fabrication methods for these materials are currently the subject of much study. High quality, transparent, low loss films must be grown for application into device structures. An important parameter in determining the quality of ferroelectric thin films is the refractive index which can be measured using several techniques including the prism coupling method. Lower than bulk values of refractive index often indicate porous, off-stoichiometry, or poor quality thin films unsuitable for devices.

Of the materials being considered for use in integrated optic switching devices, potassium niobate ranks very highly due to its very strong electro-optic effect and moderate dielectric susceptibilities. This ferroelectric has been difficult to grow in bulk crystalline form, but thin films have recently been deposited making it attractive for the integrated optic applications.

EXPERIMENTAL PROCEDURE

Potassium niobate thin films were prepared by an ion beam sputtering technique described previously.[1] Sequential deposition of very thin layers of potassium oxide and niobium oxide from potassium superoxide pressed powder and niobium metal targets resulted in the formation of the desired perovskite phase. Film composition and thickness were determined from Rutherford Backscattering (RBS) spectra. The single phase nature of the films was determined from X-ray Diffractometer (XRD) scans of the films and Selected Area Diffraction (SAD) patterns from transmission electron microscope (TEM) specimens.

Optical guided waves were launched into the thin films using a symmetrical rutile prism coupler [2] with a base angle of 60° and refractive index of 2.8659. The prism and film were clamped together to achieve a good coupling spot and the clamped assembly was mounted on a goniometer. A helium-neon laser (λ = 632.8 nm) was focused on the coupling spot at the prism-film interface. The light was polarized in order to launch only TE modes in the films. A schematic of the system is shown in figure 1. The reflected beam from the prism coupler was detected with a silicon photodiode and its signal monitored with a chart recorder. The prism coupling assembly was rotated until a sharp decrease in the reflected beam intensity was detected signaling the launching of a guided mode. The coupling angle relative to normal incidence of the input beam on the entrance face of the prism was measured. A computer was used to perform the iterative calculation necessary to determine the refractive index of the film from the coupling angle and the film thickness.[3]

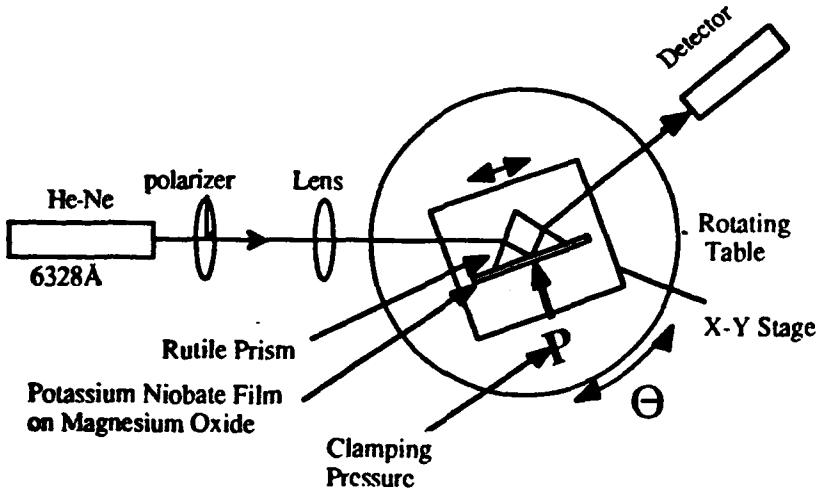

Figure 1. Prism coupling system used to determine thin film refractive index.

RESULTS AND DISCUSSION

Guided-wave characterization

Epitaxial b-axis oriented orthorhombic potassium niobate thin films were grown on single crystal magnesium oxide (001) substrates. Magnesium oxide was chosen for these experiments because of its close lattice match with $KNbO_3$ and its refractive index of 1.73. A low refractive index relative to the thin film is necessary to prevent guided-wave losses into the substrate. In addition, the crystallographic orientation of the films on MgO is suitable to make use of one of the larger coefficients of the electro-optic tensor in integrated optic devices.

The compositions of the films were analyzed using RBS spectra. Figure 2 shows a representative spectra of the $KNbO_3$ films. All films measured were slightly potassium deficient with a potassium to niobium ratio in the range of $0.85{:}1 < K{:}Nb < 0.95{:}1$. As stoichiometric potassium niobate (K:Nb = 1:1) is reached and exceeded the films roughen and change from transparent to translucent. The single phase nature and the orientation of the films can be seen from the X-ray diffraction scan shown in figure 3. The epitaxial relationship between the films and the substrate was verified from SAD patterns of TEM samples.

The refractive index of the $KNbO_3$ thin films was determined by measuring the angle at which guided modes were launched into the films using a prism coupler. Only the TE_0 mode was launched because the film thickness was in the range 2000 to 2500 angstroms, determined from the RBS spectra. The coupling angle was determined by detecting a sharp decrease in the intensity of the beam reflected from the prism-film interface as the incident angle was changed as shown in figure 4. At 632.8 nm the refractive index of the films was determined to be 2.28. This result is in good agreement with published values of the refractive index of bulk orthorhombic $KNbO_3$ and indicates that the films are dense and of high quality. For b-axis (010) oriented films, the refractive index for TE polarized optical waves should lie in the range between the refractive indices in the a-, (100), and c-, (001), crystallographic directions, 2.28 to 2.17, respectively.

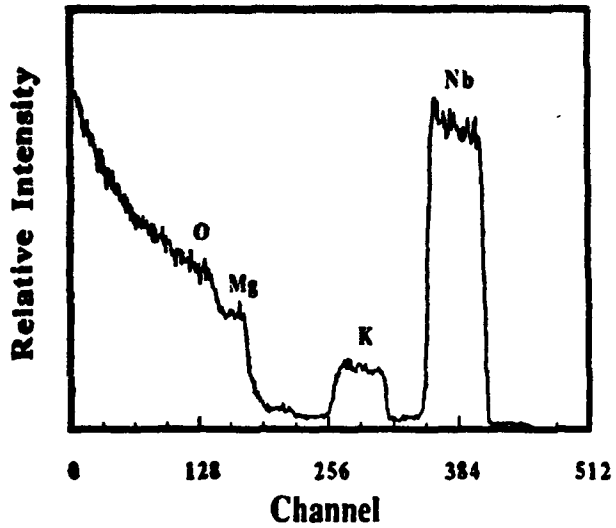

Fig. 2. Rutherford Backscattering spectra of a $KNbO_3$ thin film.

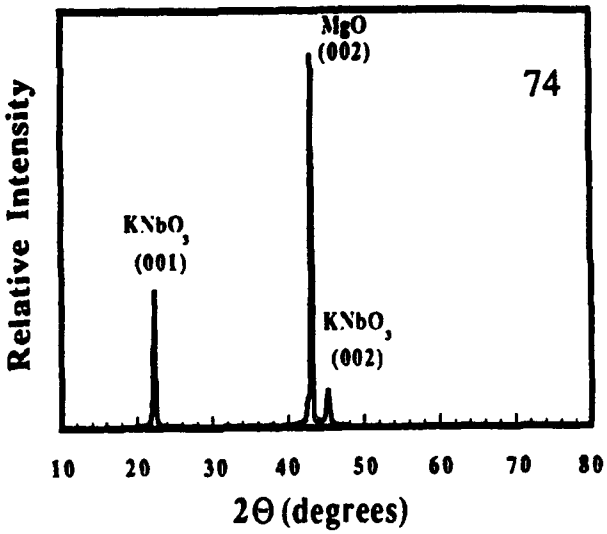

Fig. 3. X-ray diffraction scan of a $KNbO_3$ thin film.

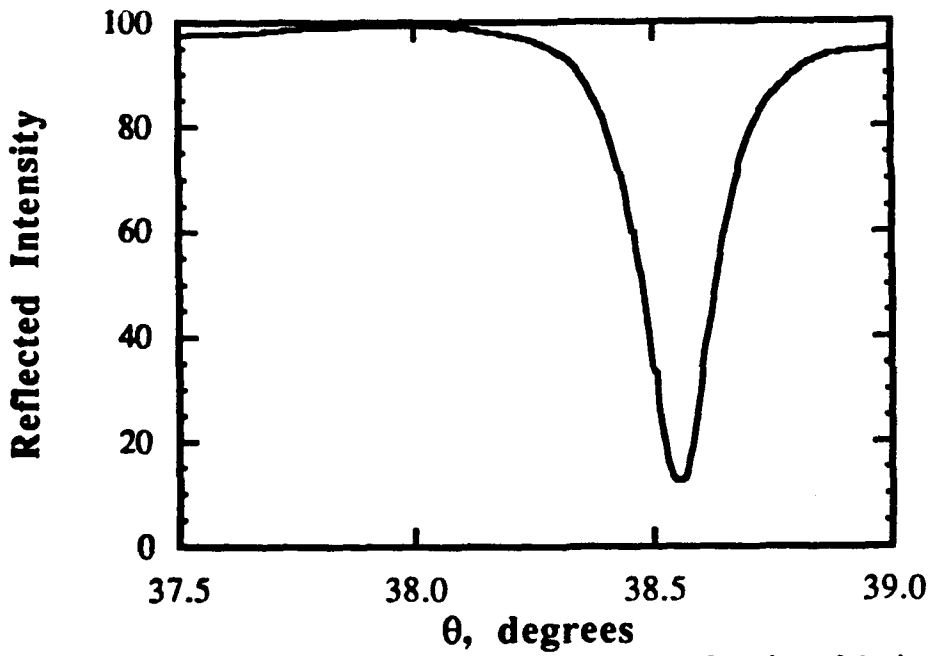

Fig. 4. The intensity of reflected light from a prism coupler as a function of the index of refraction of a propagating mode which is proportional to the angle of incidence.

$KNbO_3$ Phase Modulator Model

To demonstrate the utility of the ion beam sputter-deposited potassium niobate thin films, a waveguide electro-optic modulator based on the thin films was modeled. High quality films of $KNbO_3$ have been deposited on single crystal magnesium oxide (001). These films have been grown heteroepitaxially on the MgO surface with P_S of the orthorhombic $KNbO_3$ oriented in the plane of the film. These films will serve as the basis for the electro-optic phase modulator model. There are four equivalent directions for P_S in the plane of the film, but, for the purposes of this model, a film whose polarization vectors all point in a single direction will be considered. The results of the model will then be compared to existing technology.

The optical indicatrix for $KNbO_3$, a biaxial material, can be written as[4]

$$B_1x_1^2 + B_2x_2^2 + B_3x_3^2 + 2B_4x_2x_3 + 2B_5x_1x_3 + 2B_6x_1x_2 = 1 \qquad (1)$$

where $B_i = 1/n_i^2$, and the subscripts use contracted indices. Deformation of the optical indicatrix occurs as a result of the electro-optic effect when an electric field is applied to the crystal. Potassium niobate belongs to the crystal class mm2, so the deformation of the indicatrix obeys the relation

$$(B_1 + r_{13}E_3)x_1^2 + (B_2 + r_{23}E_3)x_2^2 + (B_3 + r_{33}E_3)x_3^2 + 2r_{42}E_2x_2x_3 + 2r_{51}E_1x_1x_3 = 1 \qquad (2)$$

For the use of the $KNbO_3$ films discussed above in guided-wave devices, light must propagate in the 1-3 plane. The guided wave may be polarized either TE (in the 1-3 plane) or TM (normal to the 1-3 plane) in a single mode waveguide. Thus, for these thin films the fourth term in Eq. (2) is of no consequence since light can not be polarized in the 4 direction.

For a field applied along x_3, Eq. (2) reduces to

$$(B_1 + r_{13}E_3)x_1^2 + (B_2 + r_{23}E_3)x_2^2 + (B_3 + r_{33}E_3)x_3^2 = 1 \qquad (3a)$$

while for a field applied along x_1, Eq. (2) becomes

$$B_1x_1^2 + B_2x_2^2 + B_3x_3^2 + 2r_{51}E_1x_1x_3 = 1. \qquad (3b)$$

Of the linear electro-optic coefficients appearing in Eqs. (3a) and (3b), r_{51} is the largest for $KNbO_3$, 105×10^{-12} m/V.[5] Utilization of this strong effect requires that a TE guided mode propagating in the 5 direction (the shear direction between the x_1 and x_3 axes) in the crystal be used. The geometry of the proposed device is shown in Fig. 5.

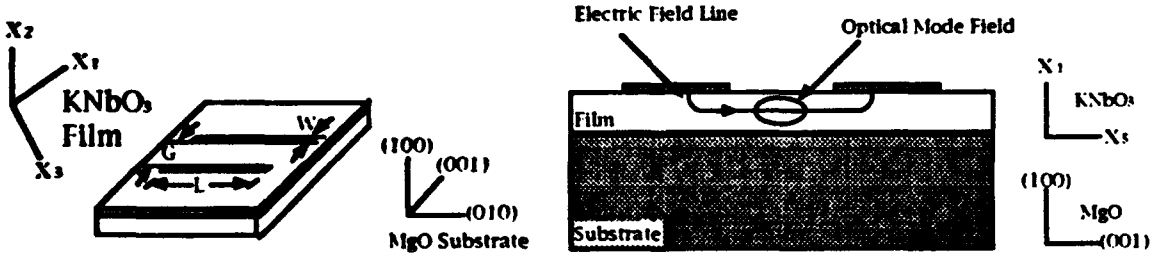

Fig. 5. Geometry of the proposed $KNbO_3$ electro-optic modulator.

The total phase shift for a TE mode propagating a distance L along the 5 direction in the film is $\Delta\beta L = 2\pi L(\Delta n_5)/\lambda$. From Eq. (3b), Δn_5 can be found to be

$$\Delta n_5 = -\tfrac{1}{2} n_5^3 r_{51} E_1 \qquad (4)$$

To determine the applied electric field, E must be determined for the electrode geometry shown in Fig. 7-1(b). The electrode geometry shown, where the horizontal field is used for modulation, has been studied in depth by several researchers[6,7,8,9], with the result that E_1 in Eq.(4) can be replaced by $\Gamma V/\sqrt{2}\,G$ where V is the applied voltage, G is the gap between the strip electrodes and Γ represents the overlap integral between the electrical and optical fields. The expression is modified by $1/\sqrt{2}$ to determine the component of the total field in the x_1 direction. The overlap integral can be calculated from

$$\Gamma = \left(\frac{G}{V}\right)\iint E|E'|^2\,\partial A \qquad (5)$$

where E is the applied electric field and E′ is the normalized optical field distribution. Using Eqs. (4) and (5), the total phase shift can be written as

$$\Delta\beta L = -\frac{\pi}{\sqrt{2}} n_5^3 r_{51} \Gamma (V/G)(1/\lambda) \qquad (6)$$

Device length and modulation voltage are two critical parameters in device design. For device optimization the product VL should be minimized. Equation (6) can be rewritten to identify the relationship between the other device parameters and the VL product. The result, using π as the desired phase shift for the modulator, is

$$VL = \frac{\sqrt{2}\lambda G}{n_5^3 r_{51} \Gamma} \qquad (7)$$

For minimization of VL, (G/Γ) must be minimized. However, Γ is a function of G and the optical mode size. Alferness[6] and Marcuse[7] have graphically presented this relationship for use in device design.

Before choosing actual device dimensions, modulation bandwidth must be considered. The modulation bandwidth when determined from the lumped electrode parameters is dependent on the electrode design and the dielectric constant of the thin film. The bandwidth is determined from $\Delta f = 1/\pi RC$ where R is the impedance of the device, typically 50 Ω (matched to the driving circuit), and C is the capacitance of the strip electrodes. For symmetric strip electrodes as shown in Fig. 5, the capacitance per unit length is[6,10]

$$\frac{C}{L} = \varepsilon_{eff} \frac{K'(r_s)}{K(r_s)} \qquad (8)$$

where $r_s = (2W/G+1)^{-1}$ and $\varepsilon_{eff} = (\varepsilon_0/2)(1+\varepsilon_S)$ is the RF dielectric constant. For $KNbO_3$ in the geometry considered here, $\varepsilon_S = \varepsilon_5 = 74$. K is the complete elliptic integral of the first kind and $K'(r_s) = K[(1-r_s^2)^{1/2}]$. Alferness[6] has graphically determined C/L and $\Delta f \cdot L$ vs. G/W for $LiNbO_3$ and the results can be scaled appropriately for $KNbO_3$.

Modulation bandwidth can also be limited by the inverse of the optical or electrical transit times. Normally, the bandwidth is limited by the electrodes and is determined as above. The bandwidth is therefore dependent on G/W, increasing as the ratio of G/W increases. However, from Eq. (7) it can be seen that a small electrode gap is required to minimize the VL product. Therefore, to maximize the modulation bandwidth requires a small electrode width. The electrical transit time cutoff frequency places a practical limit on the electrode gap to width ratio. Calculated as

$$f_t = \frac{c}{\pi(\varepsilon_{eff} L)^{1/2}} \tag{9}$$

the cutoff frequency for $KNbO_3$ is 1.5 GHz•cm and 2.2 GHz•cm for $LiNbO_3$. There is thus no advantage for G/W > 3 for a $KNbO_3$ device.

The ratio of drive voltage to modulation bandwidth can be used as a figure of merit in evaluating device design. Using Eqs. (7) and (8) presented above, the ratio is

$$V/\Delta f = \sqrt{2}\pi R\lambda\left(1/n_5^3 r_{51}\right)(G/\Gamma)(C/L) \tag{10}$$

Table 1 summarizes the device geometry and operation parameters for optimized modulators based on potassium niobate thin films and X-cut, Y-propagating titanium-diffused lithium niobate waveguides. Based upon the drive voltage to modulation bandwidth ratio and the VL product, the potassium niobate based modulator compares favorably with the lithium niobate modulator. The potassium niobate modulator uses a much larger electro-optic coefficient than the lithium niobate modulator, but the advantage gained is partially offset by the larger dielectric constant of $KNbO_3$ for the geometry considered. Based on the drive voltage to modulation bandwidth ratio, the theoretical potassium niobate modulator represents an 80% improvement over the lithium niobate modulator.

Table 1. Comparison of optimized phase modulators.

	$KNbO_3$ Thin Film	Ti-diffused $LiNbO_3$
Electro-optic Coefficient	$r_{51} = 105\times10^{-12}$ m/V	$r_{33} = 30.8\times10^{-12}$ m/V
RF Dielectric Constant, ε_S	74	35
Electrode Gap, G, (mm)	2	1
Electrode Width, W, (mm)	1	2
Wavelength, λ, (nm)	633	633
Overlap Integral, Γ	0.7	0.3
V•L Product, (V•mm)	2.2	6.4
Electrical Cutoff Freq., f_t, (GHz•cm)	1.5	2.2
RC Bandwidth•Length, Δf_{RC}•L, (GHz•cm)	1.4	2.1
$(V/\Delta f)_{min}$, (V/GHz)	0.2	0.5

Very high quality lithium niobate devices are currently being produced. However, a large market for these devices has yet to develop. One of the principle reasons for the small market is the difficulty in integrating these devices with thin film optoelectronic technology. It is in this area that thin films such as potassium niobate can excel. Several very important materials issues need to be addressed before the thin films can take the place of the bulk single crystal devices, however. High optical losses continue to plague thin film waveguides. These losses, primarily due to scattering, must be decreased to acceptable levels based upon the device being considered. In addition, for best use of the thin film materials, they must be grown on silicon or gallium arsenide. Due to the high indices of refraction of Si and GaAs, low index (<2) buffer layers must first be grown on the substrates before the electro-optic material. These buffer layers must possess a lattice suitable to match both the substrate and the electro-optic material. Work is currently in progress at North Carolina State University to grow such materials.

SUMMARY

The refractive indices of epitaxial potassium niobate (001) thin films deposited on single crystal magnesium oxide (001) have been measured using a prism coupler. The films were

fabricated using an ion beam sputter-deposition system and their compositions determined from Rutherford Backscattering spectra. The thickness of the films was in the range of 2000 to 2500Å so the films supported only one TE mode. Smooth, transparent films that were slightly potassium deficient had a refractive index of 2.28. This result falls within the expected range of 2.279 to 2.329 for bulk single crystal $KNbO_3$ with the same orientation as the films. 78

A model of an electro-optic phase modulator was developed which optimizes the drive voltage and modulation bandwidth of the device. The model was based on the epitaxial $KNbO_3$ films grown on MgO (001) using the ion beam sputter-deposition technique. The characteristics of the optimized device demonstrate the potential of $KNbO_3$ films to surpass bulk single crystal $LiNbO_3$, which is currently the material of choice for guided-wave integrated optics devices.

ACKNOWLEDGEMENTS

The authors would like to acknowledge the support of the Office of Naval Research for its support of this research program, Dr. O. Auciello, Dr. K. J. Bachmann, and Dr. S. H. Rou for useful discussions contributing to this work, and the National Defense Science and Engineering Graduate Fellowship program for their support of T. M. Graettinger.

---

[1]A. I. Kingon, S. H. Rou, M. S. Ameen, T. M. Graettinger, K. Gifford, O. Auciello, and A. R. Krauss, in *Ceramic Transactions*, vol. 14: Electrooptics and Non-Linear Optic Materials, edited by A. S. Bhalla, E. M. Vogel, and K. M. Nair (American Ceramic Society, Westerville, Ohio, 1990), pp. 179-196.

[2]P. K. Tien and R. Ulrich, J. Opt. Soc. Am. 60(10), 1325-1337 (1970).

[3]R. Ulrich and R. Torge, Applied Optics 12(12), 2901-2908 (1973).

[4]I. P. Kaminow, An Introduction to Electrooptic Devices, (Academic Press, New York, 1974), p. 25.

[5]Landolt-Bornstein, New Series, Group III (Springer, New York, 1981), Vol. 16, pt. A.

[6]R. C. Alferness, IEEE Trans. Microwave Theory Tech., MTT-23. 1121-1137 (1982).

[7]D. Marcuse, IEEE J. Quantum Electron., QE-18, 393-398 (1982).

[8]D. Marcuse, (corrections to ref. 4),IEEE J. Quantum Electron., QE-18, 807 (1982).

[9]O. G. Ramer, IEEE J. Quantum Electron., QE-18, 386-392 (1982).

[10]J. S. Wei, IEEE J. Quantum Electron., QE-13, 152-158 (1977).